A NOVEL APPROACH FOR THE RAPID ESTIMATION OF DRAINAGE VOLUME, PRESSURE AND WELL RATES

A Thesis

by

NEHA GUPTA

Submitted to the Office of Graduate Studies of
Texas A&M University
in partial fulfillment of the requirements for the degree of

MASTER OF SCIENCE

Approved by:

Chair of Committee,	Michael J. King
Committee Members,	Akhil Datta-Gupta
	Richard L. Gibson
Head of Department,	Dan Hill

December 2012

Major Subject: Petroleum Engineering

ABSTRACT

For effective reservoir management and production optimization, it is important to understand drained volumes, pressure depletion and reservoir well rates at all flow times. For conventional reservoirs, this behavior is based on the concepts of reservoir pressure and energy and convective flow. But, with the development of unconventional reservoirs, there is increased focus on the unsteady state transient flow behavior. For analyzing such flow behaviors, well test analysis concepts are commonly applied, based on the analytical solutions of the diffusivity equation. In this thesis, we have proposed a novel methodology for estimating the drainage volumes and utilizing it to obtain the pressure and flux at any location in the reservoir.

The result is a semi-analytic calculation only, with close to the simplicity of an analytic approach, but with significantly more generality. The approach is significantly faster than a conventional finite difference solution, although with some simplifying assumptions. The proposed solution is generalized to handle heterogeneous reservoirs, complex well geometries and bounded and semi-bounded reservoirs. Therefore, this approach is particularly beneficial for unconventional reservoir development with multiple transverse fractured horizontal wells, where limited analytical solutions are available.

To estimate the drainage volume, we have applied an asymptotic solution to the diffusivity equation and determined the diffusive time of flight distribution. For the pressure solution, a geometric approximation has been applied within the drainage volume to reduce the full solution of the diffusivity equation to a system of decoupled ordinary differential equations. Besides, this asymptotic expression can also be extended to obtain the well rates, producing under constant bottomhole pressure constraint.

In this thesis, we have described the detailed methodology and its validation through various case studies. We have also studied the limits of validity of the approximation to better understand the general applicability. We expect that this approach will enable the inversion of field performance data for improved well and/or fracture characterization, and similarly, the optimization of well trajectories and fracture design, in an analogous manner to how rapid but approximate streamline techniques have been used for improved conventional reservoir management.

DEDICATION

To my parents and brother

ACKNOWLEDGEMENTS

First and foremost, I would like to thank my committee chair, Dr. Michael King, who has been a great advisor and mentor. I would also like to extend my gratitude to my other committee members, Dr. Akhil Datta-Gupta and Dr. Richard Gibson, for their guidance during the course of this research.

During this work, I have worked and learnt a lot from my MCERI research group students, so I would like to thank them and also to MCERI for funding my research. The courses during my Master's program and all the professors have been very helpful for this work. So I am thankful to all my friends, colleagues and the department faculty and staff for their support and for making my stay at Texas A&M University so memorable.

Last but definitely not the least, I'm thankful to my parents and my brother who have loved and cared for me in every phase of life and made me who I am.

NOMENCLATURE

A_n	Flow surface area for n^{th} dimension
B_o	Formation volume factor of oil
bpd	Barrels per day
c_t	Total compressibility
c_r	Conversion coefficient
D_{ij}	Gradient for diffusive time of flight
k	Permeability
n	Dimension
P	Pressure
P_i	Initial reservoir pressure
P_{wf}	Well bottomhole pressure
$\Delta P'$	Pressure derivative
Q_w	Production rate for well
r_{inv}	Radius of investigation
r_w	Wellbore radius
t	Production time
T	Dimensionless time
V_p	Reservoir drainage volume
x_f	Fracture half length

Greek variables

α	Diffusivity
τ	Diffusive time of flight
μ	Viscosity of fluid
ϕ	Porosity
ξ	Dimensionless radius
ω	Frequency of wave
θ_i	Incident angle
θ_r	Reflected angle
θ_t	Transmitted angle

Abbreviations

CMG	Computer Modeling Group
FMM	Fast Marching Method
MTFW	Multiple Transverse Fractured Well
SRV	Stimulated Reservoir Volume

TABLE OF CONTENTS

Page

LIST OF FIGURES

Page

LIST OF TABLES

Page

CHAPTER I

INTRODUCTION AND LITERATURE REVIEW

Chapter I provides a preface to the research work done for this thesis. It explains the necessity of the conducted research, the previous work done in this area and the main objectives of our research.

1.1 Research background

With increasing scarcity of conventional oil & gas resources, unconventional reservoirs have become the best prospective energy resource, especially in the United States. For the economic development of such reservoirs, improved exploitation techniques like horizontal drilling and hydraulic fracturing have played a key role, by creating a stimulated reservoir volume (SRV). The SRV represents the maximum reservoir volume contributing to production in such reservoirs typically developed with Multiple Transverse Fractured Wells (MTFW) as shown in **Fig. 1**. In order to maximize economic benefit, it is critical to optimize the SRV and the produced volume by improving fracture design and well placement in the reservoir.

To achieve this goal, it is necessary to understand the impact of varying fracture designs and well placement. Also, it is important to predict the production rates obtained and the pressure depletion behavior in the reservoir to optimize the production. This provides us the basis of our research, which was to devise a rapid and efficient approach for the

prediction of drainage volume, pressure and rate in a heterogeneous reservoir system, useful for sensitivity analysis and production optimization.

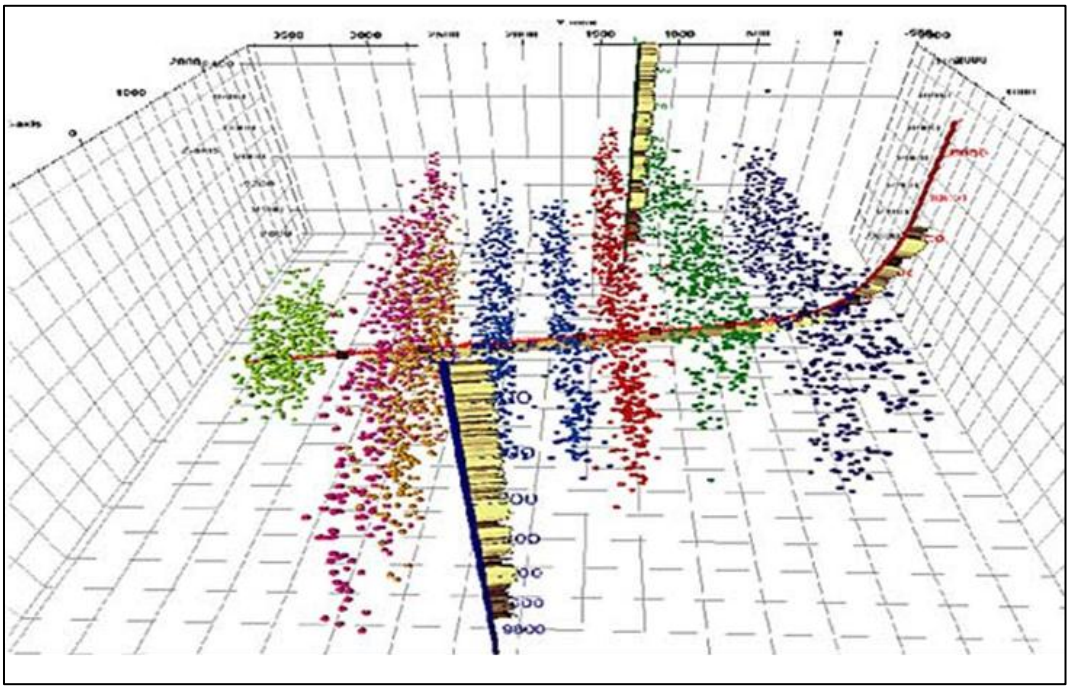

Fig. 1—Stimulated reservoir volume of a multiple transverse fractured well

The currently available techniques for estimating drainage volumes and pressure and rate behavior are either analytical solutions or numerical simulation. The analytical solutions include pressure transient analysis and production rate analysis, but these are generally restricted to homogeneous reservoirs, simple well geometries and specific well locations. For unconventional reservoirs, which are generally heterogeneous in nature and have complex well geometries, the typical analytical solutions for transient and boundary dominated flow cannot be directly applied. To handle such reservoirs, one approach is to

conduct numerical simulations but these can be cumbersome and time consuming, especially within optimization studies and sensitivity analysis of large reservoir models.

Therefore, in our research work, we have developed a novel semi-analytical approach. It requires the reservoir property model as input, and provides a rapid estimation of the reservoir drainage volume and the pressure and rate response, without a conventional numerical simulation. In order to deal with a generalized reservoir system, this solution has the capability of handling heterogeneity, bounded or semi-bounded reservoir systems and complex well geometries with arbitrary locations in the reservoir.

We expect that such an approach will also be beneficial in reserves estimation, infill targeting in multi-well reservoirs and inversion of field performance data for improved well or fracture characterization. It should enable the optimization of well trajectories and fracture design, in an analogous manner to how rapid but approximate streamline techniques have been used for improved conventional reservoir management.

1.2 Literature review

In this section, we would review the existing analytical solutions for pressure transient analysis, drainage volume estimation and production data analysis, which have mostly been developed for homogeneous reservoirs. We will also discuss their applications as well as limitations to emphasize the need of the current research work.

Pressure Transient Analysis (PTA) is fundamental for understanding conventional as well as unconventional reservoir behavior. These analytical solutions have been well developed and widely applied in the industry for conventional reservoirs, but they are gaining special significance for unconventional reservoirs. For conventional reservoirs, the transient and steady state well test solutions are usually developed for radial well, homogeneous reservoir properties and simple boundary locations and conditions (Lee 1982). Their most common application is to estimate the reservoir properties and detect the presence or location of boundaries from a given well test response. For drainage volume estimation in such cases, the general approach is to use the concept of 'radius of investigation'.

The radius of investigation is defined as the maximum radius in a homogeneous formation in which the pressure has been affected due to the impulse created at the well when opened or shut-in. Several authors have estimated the value for the radius of investigation and Kuchuk (2009) has summarized these definitions. However, the most widely used definition in the industry is the one given by Dr. Lee, which denotes the radius at which the pressure derivative is maximum in the reservoir. The basic relation derived by dimensional analysis shows that it is dependent on the diffusivity of the formation and the time from the start of impulse (**Section 2.1**).

Recently, Kuchuk (2009) provided a detailed analysis of the radius of investigation for radial cylindrical wells in homogeneous reservoirs. In this work, he made an important

observation that the coefficient value also varies with different boundary conditions like presence of faults or other boundary shapes. Based on the pressure responses of some simple cases, he analytically calculated the boundary distances and time of deviation from the infinite reservoir behavior and then compared with the actual data. No one particular coefficient was found to obtain the correct results for all cases. Besides this observation, he introduced some new equations to show the dependency of the radius of investigation on production rate, formation thickness and the gauge resolution in radial cylindrical systems. But they were meant only for early flow times and for specific well and reservoir boundary locations. Additionally, he also investigated the impact of variable rate, wellbore storage and skin on the radius of investigation. He recognized that the wellbore storage only affected the early flow time calculations and the skin did not have any significant impact on the estimation of radius of investigation.

Besides the works summarized by Kuchuk, another interesting approach was introduced by Nordbotten et al. (2004) for determining the outer boundary of the propagating pressure wave in a radial cylindrical system. This solution was developed for estimating the leakage volume in water reservoirs. The derivation is based on the infinite series approximation of the well function used in the transient pressure solution. Based on the number of terms used in the expansion, a cut-off value for the radial distance can be used as a definition of the outer boundary, beyond which the pressure drop is considered negligible. For all cases, the outer boundary was determined to be a function of the square root of time, similar to our definition of the radius of investigation.

Apart from the radius of investigation concept, an alternative method for estimating the drainage volume variation in a finite reservoir was recently suggested by Agarwal (2010). This approach can determine the reservoir drainage volume as well as the average reservoir pressure at all flow times, based on the reservoir material balance concepts. The main limitation of this approach is that it is only suitable for a radial well in a homogeneous reservoir and it requires the well test pressure response as an input to predict the drainage volume variation.

As stated, all of the above-explained approaches have a major limitation that they are only suitable for radial cylindrical wells. But it is well known that unconventional reservoirs are generally developed with vertical or horizontal wells with hydraulic fractures. So it becomes important to understand the transient behavior of hydraulically fractured wells. Since hydraulic fracturing has been a major stimulation method in the industry since 1949, there is a lot of literature work available for related studies (Cinco-Ley and Samaniego-V 1981; Raghavan et al. 1972; Riley et al. 1991).

Initially, hydraulic fracturing was introduced to enhance the oil & gas production from vertical wells in conventional reservoirs but it had significant impact on the development of unconventional reservoirs. Combined with horizontal well drilling, multi-staged transverse hydraulic fractures have proven to be the best technology so far, for maximizing the reservoir drainage volumes and the ultimate recovery in low permeability reservoirs. Meyer et al. (2010) has recently summarized the major

contributions in the study of multi fractured horizontal wells in shale gas reservoirs. These comprise of the analytical solutions and numerical models developed so far, to improve the understanding of the flow regimes and for optimization and production forecast purposes. Song et al. (2011) has also explained the major flow regimes for such wells and has presented a well design approach including adsorption effects for maximizing economic benefit. From these works (Al-Kobaisi et al. 2006; Bello and A 2010; Meyer et al. 2010; Song et al. 2011), some commonly identified flow regimes for such wells are fracture storage dominated flow, pseudo-linear flow normal to transverse fractures, pseudo-radial flow in the case of large spacing between fractures and pseudo pseudo-steady state flow which indicates that the SRV has been reached.

The pressure transient solutions are generally based on the assumption that the well is producing at constant production rates. So these solutions are only applicable in the initial stages of production, when the well is producing at its peak with constant production rates. After this, the production rate starts declining and the operational constraint is shifted to a constant minimum well bottomhole pressure (BHP). For analyzing the well in the declining phase with constant BHP, production data analysis (PA) concepts have been applied for understanding well behavior. Similar to PTA, PA is also commonly used for estimating reservoir properties from a given well production rate and BHP response and for reserves estimation.

For any well, be it radial-cylindrical or fractured, all the existing analytical approaches for pressure and rate analysis have a major drawback of being limited to homogeneous reservoirs, constant reservoir and fluid properties, single phase flow, idealized well and reservoir geometries, specific well locations in the reservoir or fixed boundary conditions. There are different solutions available for specific cases with certain flow period restrictions but there seems to be a lack of a common solution that can provide results at all flow times for any reservoir system.

The only available option to handle other complications like reservoir heterogeneity, complex bounded reservoirs, different well geometries and arbitrary well locations is to use numerical simulation. But simulation can be cumbersome and time-consuming to predict the drainage volumes, flow regimes and pressure & rate variations at all times. Therefore, a simpler approach with a hybrid modeling technique has been developed in this work to enable faster and efficient problem solving.

1.3 Introduction to the thesis work

As explained in the previous sections, the main objective of this project was to develop a novel approach to predict the drainage volume, pressure and rates at all times. In order to develop a general solution, this method was designed to remove the limitations in previous approaches like heterogeneity, bounded or semi-bounded reservoir systems, complex well geometries and arbitrary well locations in the reservoir. A brief summary of the work done for this thesis has been provided in this section. This includes the

theory and methodology of the proposed solution (Chapter II & III), case studies for illustration purposes, their results, and discussion section for validation of the method (Chapter IV). The results are summarized in the conclusions (Chapter V).

In chapter II, we will discuss the analytical solutions for the diffusivity equation in homogeneous reservoirs (**Section 2.1**) and then explain the methodology of extending the solution to heterogeneous reservoirs. This method can be applied to estimate the 'depth of investigation' and the drainage volume at all flow times in homogeneous and heterogeneous reservoirs with different well geometries (**Section 2.3**).

Then in the next chapter (III), we will describe the generalized pressure transient and rate transient solutions by using a geometric approximation. For accurate calculations using the geometric approximation, the asymptotic pressure and flux boundary solutions have also been explained. Another crucial thing to generalize the solution to heterogeneous reservoirs is to consider the validity and limitations of the assumptions used for pressure front propagation across media boundary, as explained in **Section 3.1.2**.

To illustrate the proposed methodology, several examples of homogenous and heterogeneous cases have been studied in Chapter IV. The results for drainage volume, pressure and rate variations have also been shown. These results have been validated by comparisons with available analytical solutions and simulation results. Finally, the

conclusions from the above work and the recommendations for further studies have been summarized in Chapter VI.

As shown in the coming sections, this novel semi analytical approach is rapid and provides good approximate solutions, improving our ability to evaluate multiple scenarios and for improved reservoir management. The ultimate purpose of this approach is to facilitate Stimulated Reservoir Volume (SRV) estimation, well and fracture placement optimization, reserves evaluation, infill targeting and inversion of real field performance data for well/fracture characterization in unconventional reservoirs. Some works have already been published based on the application of this methodology (Datta-Gupta et al. 2011; Kang et al. 2011; Xie et al. 2012)

CHAPTER II

METHODOLOGY OF ESTIMATING DRAINAGE VOLUME

This chapter first describes the basic concept of radius of investigation in homogeneous reservoirs, used to estimate the investigated reservoir volume during a well test or the reservoir drainage volume during production. Assuming radially symmetric flow in homogeneous reservoirs, the diffusivity equation has also been solved analytically to provide the radius of investigation as well as the general pressure and flux solutions for any dimension.

In order to solve the diffusivity equation for heterogeneous reservoirs, an asymptotic solution has been derived (Vasco et al. 2000), analogous to some other wave theories. When only the high frequency term in this solution is considered, an Eikonal equation is obtained which governs the pressure front propagation from a source point to any location in a general reservoir system. This equation can be solved very efficiently by using an algorithm known as the 'Fast Marching Method', hence expediting the calculations tremendously (Datta-Gupta et al. 2011; Xie et al. 2012).

The solution from this algorithm provides a 'diffusive time of flight' distribution, which can then be converted to actual time distribution for pressure front propagation away from the source well. This time distribution can be used as time contours indicating the location of the pressure wave at that particular time and thus provides a quick

visualization of the 'Depth of Investigation' in the reservoir. Once the location of the pressure wave front is known at all times, the cumulative pore volume of the cells encompassed by it can be used to calculate the Drainage Volume.

2.1 Radius of investigation in homogeneous reservoirs

When a well starts producing from a reservoir at initial conditions or when a well is shut in for a well test, there is an impulse created at the well which generates pressure waves which propagate into the reservoir. For a radial well with infinitesimal wellbore in an infinite and isotropic reservoir, producing at constant production rates, the radius up to which the pressure wave has propagated at any time is given by the term 'radius of investigation'. This concept has been used in the industry for decades and several definitions have been associated to this, well summarized by Kuchuk (2009). However, the most common definition used in the industry was given by Lee (1982) which denotes the radius at which the pressure derivative is maximum. It is defined by the following **Eq. (1)**:

$$r_{inv} = \sqrt{\frac{c_r k t}{\phi \mu c_t}} \tag{1}$$

where,

r_{inv}, radius of investigation (ft);

k, permeability (md);

t, time (hours);

ϕ, porosity (fraction);

μ, viscosity (cp);

c_t, total compressibility (fluid plus rock) and

c_r, the conversion coefficient depending on the flow geometry, eg., linear (c_r=2), radial (c_r=4) or spherical (c_r=6).

As seen in **Eq. (1)**, this investigation radius depends on the time of production and on the fluid and rock properties; but is independent of the production rate. This concept is generally used for a constant producing rate well and the coefficient value used for radial flow is 4, as derived by Dr. Lee. For a well with variable production rates, the coefficient changes as shown by Kuchuk (2009) and Hsieh et al. (2007).

2.1.1 Analytical solution of the diffusivity equation

For a homogeneous reservoir with constant rock properties (porosity, permeability, reservoir thickness and rock compressibility) and single phase fluid with constant properties (viscosity and compressibility), the diffusivity equation in terms of pressure (P) and Darcy flux (Q) can be written as **Eq. (2)**:

$$A\phi c_t \frac{\partial P}{\partial t} = \frac{\partial Q}{\partial r} \tag{2}$$

The flux term, Q is defined by Darcy's law as **Eq. (3)**:

$$Q = \frac{kA}{\mu}\frac{\partial P}{\partial r} \tag{3}$$

where,

A, cross sectional area for flow (radially symmetrical);

P, pressure at any location ‘r’ and time t, and

Q, Darcy flux.

The flow cross sectional area for a radially symmetric flow can be simplified as written in the form of $A = A_o r^n$, where n= 0, 1, 2 for linear, cylindrical and spherical flow respectively. The value of A_o is a constant for linear flow, $2\pi h$ for radial cylindrical flow and 4π for spherical flow.

Combining the above two equations 2 and 3, the diffusivity equation can be written in terms of pressure as **Eq. (4)**:

$$\frac{\phi \mu c_t}{k}\frac{\partial P}{\partial t} - \frac{1}{A}\frac{\partial}{\partial r}\left(A\frac{\partial P}{\partial r}\right) = 0 \tag{4}$$

Or alternatively, in terms of the flux as **Eq. (5)**:

$$\frac{\phi \mu c_t}{k}\frac{\partial Q}{\partial t} - A\frac{\partial}{\partial r}\left(\frac{1}{A}\frac{\partial Q}{\partial r}\right) = 0 \tag{5}$$

These equations have to be solved with the following initial and boundary conditions, which assume a line (or point) source approximation for the well, when the well is producing at constant rates from an infinite acting reservoir.

Initial Conditions (t=0):

$P=P_i$, $Q=0$, $\Delta P=P_i-P=0$.

Boundary Conditions (t>0):

Well ($r = r_w \to 0$): $P = P_{wf}\,; Q = Q_w\,; \Delta P_{wf} = P_i - P_{wf}$

Far Field ($r \to \infty$): $P \to P_i; Q \to 0; \Delta P \to 0$

Eq. (5) can be solved for the flux by applying these initial and boundary conditions. It can then be integrated to obtain the pressure from **Eq. (3)**. For the solution, three new variables, T, ξ and m have been introduced for simplification as explained in **Eq. (7) to (9)**. **Eq. (5)** can be transformed to obtain the flux equation as **Eq. (6)**:

$$\left(\xi^{-m}\frac{dQ}{d\xi}\right)+\frac{d}{d\xi}\left(\xi^{-m}\frac{dQ}{d\xi}\right)=0 \tag{6}$$

where,

$$m=\frac{n-1}{2} \tag{7}$$

$$T=\frac{kt}{\phi\mu c_t} \tag{8}$$

$$\xi=\frac{r^2}{4T} \tag{9}$$

Eq. (6) can be integrated to obtain the flux solution. The radius of investigation can be obtained directly from **Eq. (6)** without an explicit solution, solving for the maximum pressure derivative, i.e., where the second derivative is zero. In terms of the new variables we get **Eq. (10)**:

$$\frac{\partial^2 P}{\partial T^2}=-\frac{\mu r}{2kAT^2}\left(\frac{dQ}{d\xi}\right)(1+m-\xi)=0 \tag{10}$$

Therefore by equating (1 + m – ξ = 0), the solutions for the radius of investigation can be obtained for different flow dimensions, as shown in **Table 1**. From these results, we

conclude that the coefficient value is 2 for linear flow, 4 for radial (cylindrical) flow and 6 for spherical flow.

Table 1. Summary of radius of investigation for different flow types

Flow Type	n	m	r_{inv}^2	T
Linear Flow	0	-1/2	2T	1/2 r_{inv}^2
Radial Cylindrical Flow	1	0	4T	1/4 r_{inv}^2
Spherical Flow	2	½	6T	1/6 r_{inv}^2

By using the same equations, the expression for the well test derivative can also be derived as **Eq. (11)**:

$$\Delta P' = -t\frac{dP}{dt} = \frac{\mu}{2^n kA_n} T^{-m}\left(-\frac{dQ}{d\xi}\right) \tag{11}$$

This equation shows that the log-log plot of pressure drop with time will have the slope of -m (**Table 1**). The slope value is 0.5 for linear flow, 0 for radial flow and -0.5 for spherical flow, which has been well used in the industry for analyzing pressure transient data to determine flow type. Thus, these results substantiate the accuracy of the derivation too.

Coming back to the solution of **Eq. (6)**, it can provide the flux solution for a radially symmetric flow in any dimension n, by using the incomplete gamma function as **Eq. (12)**:

$$Q = Q_w \frac{\Gamma(m+1,\xi)}{\Gamma(m+1)} \tag{12}$$

Once the general flux solution is obtained, it can be integrated to obtain the general pressure solution as **Eq. (13):**

$$\Delta P(r,T) = \frac{\mu Q_w}{2kA_n} \frac{r^{1-n}}{\Gamma(m+1)} .\Gamma(m, \frac{r^2}{4T}) = 0 \tag{13}$$

Although the flux is always a self-similar solution, the same is only true for the pressure solution for cylindrical flow. The specific pressure and flux solutions for linear, cylindrical and spherical flow can be obtained by using the corresponding values of m and n, as shown in **Table 2**. The flux solution for linear, radial and spherical flow as a function of dimensionless variable ξ has been shown in **Fig. 2**. The pressure drop was also calculated as a function of dimensionless time for these flow types as shown in **Fig. 3**. The pressure profile for radial flow as a function of actual time has been shown in **Fig. 4**, which shows the expanding radius of investigation.

Table 2. Specific pressure and flux solutions for linear, radial and spherical flow

Flow Type	n	m	Q/Q_w	$\Delta P(r,T)$
Linear	0	-1/2	$erfc\left(\sqrt{\xi}\right)$	$\frac{\mu Q_w}{kA}\left\{\frac{2\sqrt{T}}{\sqrt{\pi}} e^{-r^2/4T} - r \cdot erfc\left(\frac{r}{2\sqrt{T}}\right)\right\}$
Radial	1	0	$\exp(-\xi)$	$\frac{\mu Q_w}{4\pi kh} Ei\left(\frac{r^2}{4T}\right)$
Spherical	2	+1/2	$2\sqrt{\frac{\xi}{\pi}} e^{-\xi} + erfc\left(\sqrt{\xi}\right)$	$\frac{\mu Q_w}{4\pi k} \frac{1}{r} erfc\left(\frac{r}{2\sqrt{T}}\right)$

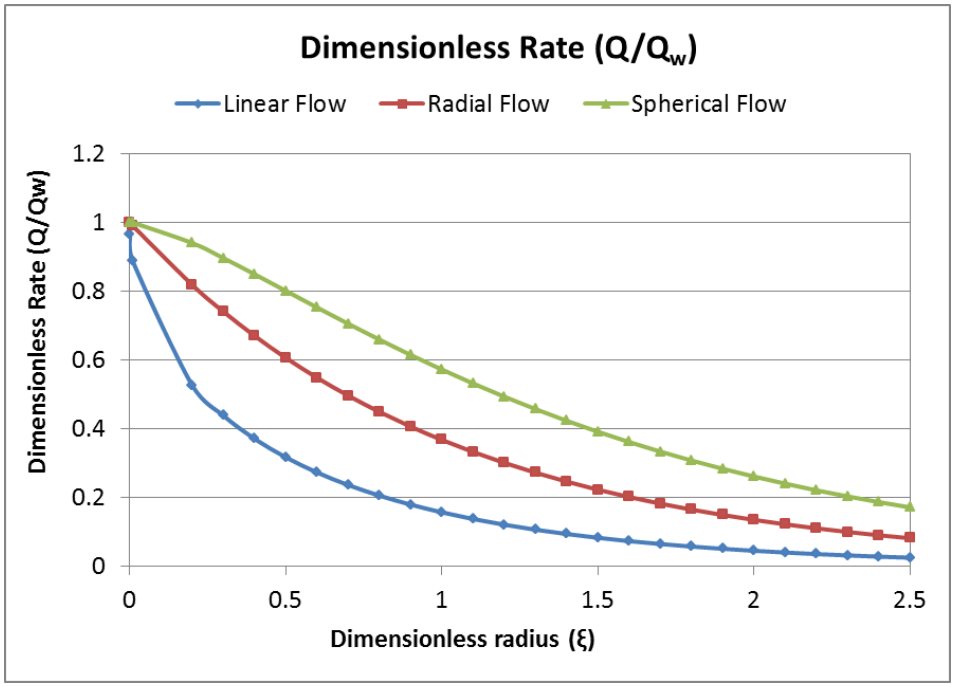

Fig. 2—Variation of flux as a function of dimensionless radius for linear, radial and spherical flow

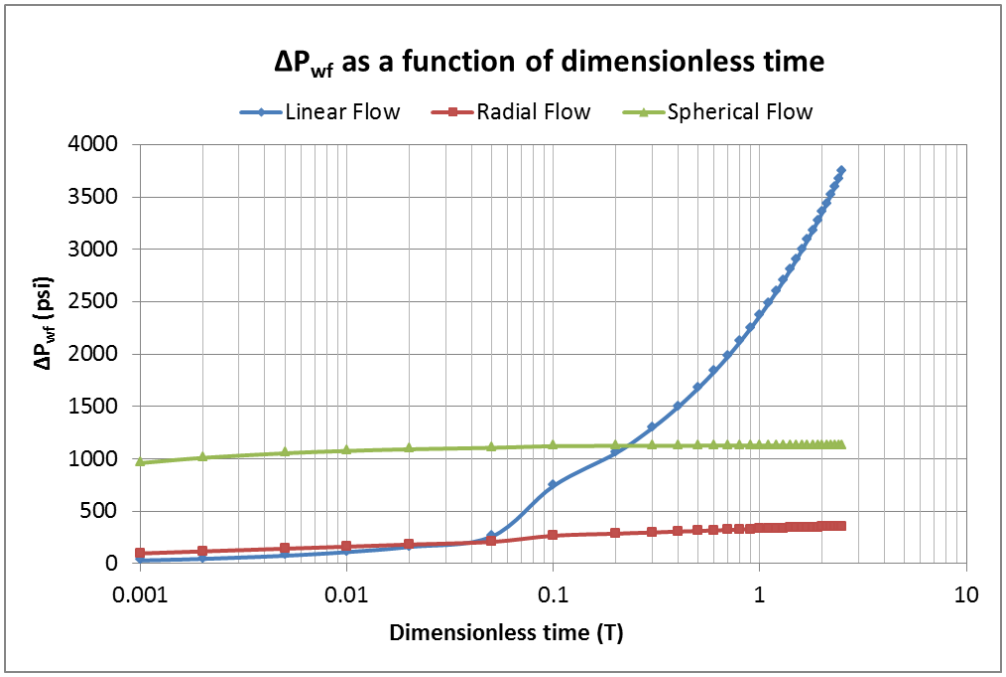

Fig. 3—Pressure drop at the wellbore as a function of dimensionless time for linear, radial and spherical flow

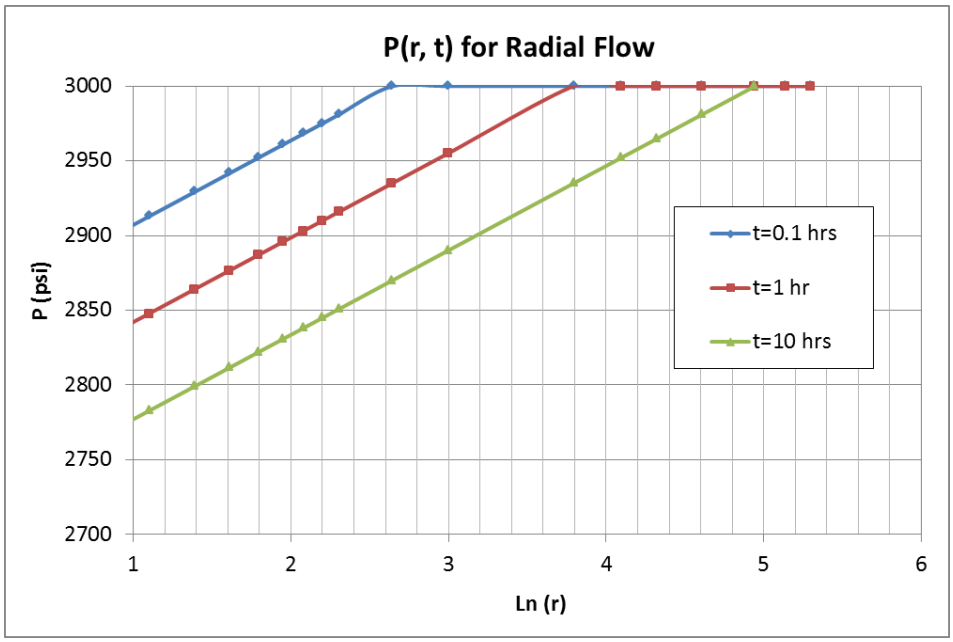

Fig. 4—Pressure profile for radial flow

2.2 Asymptotic solution of the diffusivity equation

Since the radius of investigation is only applicable for homogenous reservoirs, a generalized solution needs to be derived for heterogeneous reservoirs. In heterogeneous reservoirs, since the pressure front is not expected to be uniform in all directions, we will use the term "depth of investigation", instead of "radius of investigation", as more representative for such systems. To obtain the depth of investigation, an asymptotic solution for the diffusivity equation has been obtained (Datta-Gupta and King 2007; Vasco et al. 2000). This approach has been applied earlier in optical, medical and geophysical imaging (Virieux et al. 1994).

The derivation begins with the three dimensional diffusivity equation for a heterogeneous system, with variable porosity ($\phi(x)$) and permeability ($k(x)$) but constant fluid properties, viscosity (μ) and compressibility (c_t). It can be written as **Eq. (14)**:

$$\phi(x)\mu c_t \frac{\partial P(x,t)}{\partial t} = \nabla.\left(k(x)\nabla P(x,t)\right) \tag{14}$$

Now, by applying a Fourier transform to this equation, it becomes the following in the frequency domain as **Eq. (15)**:

$$\phi(x)\mu c_t(-i\omega)\tilde{P}(x,\omega) = k(x)\nabla^2\tilde{P}(x,\omega) + \nabla k(x).\nabla\tilde{P}(x,\omega) \tag{15}$$

The asymptotic solution to this equation can be obtained by considering the following pressure solution in terms of inverse powers of $\sqrt{-i\omega}$ as **Eq. (16)**.

$$\tilde{P}(x,\omega) = e^{-\sqrt{-i\omega}\tau(x)}\sum_{j=0}^{\infty}\frac{A_j(x)}{\left(\sqrt{-i\omega}\right)^j} \tag{16}$$

where, $\tau(x)$ is the propagation time of the pressure 'front' (also called 'Diffusive Time of Flight') and $A_j(x)$ is the pressure amplitude at the j-th order.

The leading order high frequency term in the asymptotic expansion determines the pressure front propagation, as seen in the asymptotic solutions for electromagnetic and other wave equations. The solution is written as **Eq. (17)**.

$$\tilde{P}(x,\omega) = A_o(x)e^{-\sqrt{-i\omega}\tau(x)} \tag{17}$$

By substituting this solution in **Eq. (15)** and collecting the terms with the highest order ($-i\omega$), **Eq. (18)** can be obtained for the pressure front propagation.

$$\sqrt{\alpha(x)}\left|\nabla\tau(x)\right|=1 \tag{18}$$

Here α(x) stands for diffusivity and can be defined by **Eq. (19)**

$$\alpha(x)=\frac{k(x)}{\phi(x)\mu c_t} \tag{19}$$

The above equation is in the form of an Eikonal equation and indicates that the pressure front propagates in the reservoir with a velocity of $\sqrt{\alpha(x)}$, i.e. the square root of diffusivity.

The diffusive time of flight term τ(x), is indicative of the distance travelled by the pressure front in the reservoir, away from the source. It is proportional to the square root of actual time as $\tau=\sqrt{c_r t}$, also consistent with the scaling behavior of the pressure equation. The coefficient term is dependent on the dimension of the system as explained in **Table 1**. For any given reservoir and well system, the flow regime may vary with time and so may the conversion coefficient. To capture this variation, an approach has been developed in **Section 2.3.1**, to determine the conversion coefficients. The methodology for solving **Eq. (18)** for heterogeneous reservoirs and then applying it to estimate the drainage volume is explained in the next section.

2.3 Estimation of the drainage volume by using the diffusive time of flight

To estimate drainage volume at any given time, we calculate the reservoir volume which has experienced a pressure variation caused by the impulse at the source, or in other

words, the reservoir volume encompassed by the pressure front at that time. The Eikonal equation (**Eq. 18**) governing the pressure front propagation for a general reservoir system can be solved by a very efficient front tracking method called the Fast Marching Method (Sethian 1999). This approach considers the pressure wave as a monotonically advancing front and uses a minimization algorithm to estimate the arrival time for the pressure front at any location in a reservoir.

This method has been explained in this section by using a rectangular orthogonal mesh grid, where finite difference scheme can be applied to calculate the gradient. By discretizing the above Eikonal equation on rectangular grids, we obtain the following form as in **Eq. (20)**,

$$\max\left(D_{ij}^{-x}\tau,0-D_{ij}^{+x}\tau,0\right)^2+\max\left(D_{ij}^{-y}\tau,0-D_{ij}^{+y}\tau,0\right)=1/\alpha(x)^2 \tag{20}$$

The term D represents the gradient approximated with 1st order upwind finite difference scheme, calculated in the positive and negative x & y directions as in **Eq. (21a) to (21d)**:

$$D_{ij}^{-x}=\frac{\tau_{i,j}-\tau_{i-1,j}}{\Delta x} \tag{21a}$$

$$D_{ij}^{+x}=\frac{\tau_{i+1,j}-\tau_{i,j}}{\Delta x} \tag{21b}$$

$$D_{ij}^{-y}=\frac{\tau_{i,j}-\tau_{i,j-1}}{\Delta y} \tag{21c}$$

$$D_{ij}^{+y}=\frac{\tau_{i,j+1}-\tau_{i,j}}{\Delta y} \tag{21d}$$

This discretization results in a quadratic function for the arrival time $\tau(x)$, which can be solved very efficiently.

The key to the Fast Marching Methods lies in the observation that the upwind approximation possesses a specific causality relationship. By 'causality', we mean that the solution of **Eq. (20)** at each node depends only on the smaller adjacent values. Thus, we need to solve it concurrently in the order of increasing values of T (Sethian and Vladimirsky 2000).

Fig. 5 (Xie et al. 2012) is a schematic to illustrate the FMM, where the well location is first labeled as 'accepted' points (τ=0). Their adjacent nodes are labeled as 'neighbor' points and the rest nodes are called 'far-away' points. Now to calculate the arrival time at each point, the following procedure is applied:

1. Start from the 'accepted' points,
2. Calculate the arrival time of their 'neighbor' points (A, B, C, D, etc.) using the finite difference approximation
3. Pick the minimum arrival time in the current 'neighbor' points,
    - Label it as 'accepted' (e.g., Point A in **Fig. 5b**)
    - Add its neighbors that are in 'far-away' as 'neighbors', (e.g., Points E, F & G in **Fig. 5d**)
4. Repeat steps 2 and 3 until all the points in the domain are labeled as 'accepted'.

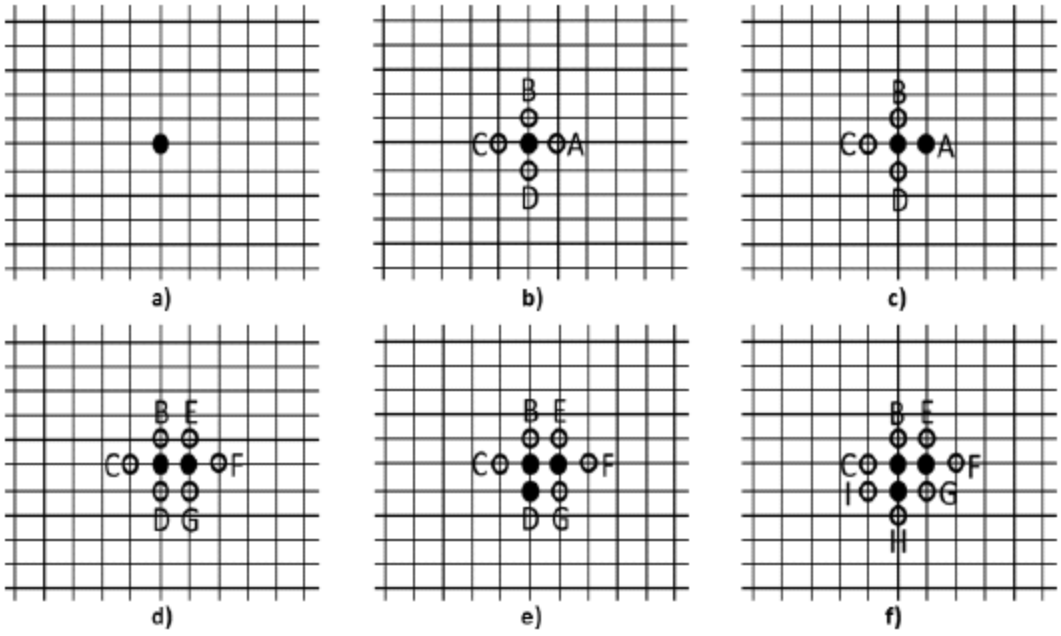

Fig. 5—Schematic description of the fast marching method showing the propagation of pressure waves in an orthogonal mesh grid

By applying the FMM approach, once the arrival time for each node has been estimated in terms of diffusive time of flight, these times can be used as contours representing the corresponding pressure front location. The study of this approximation is the fundamental purpose of this dissertation. Therefore, the drainage volume at any time can easily be calculated by summing up the pore volumes of the mesh grids inside that time contour. For these calculations of drainage volumes, we can either use the diffusive time of flight contour or the actual time contours. If the flow type in the reservoir is symmetrical and known, the diffusive time of flight can be converted to actual time by using the corresponding conversion coefficient. If not, we provide an approach for estimating the conversion coefficient in a general reservoir system in **Section 2.3.1**. But

overall, the drainage volume calculation can be expressed in simple mathematical terms as **Eq. (22)**,

$$V_p(t) = \sum_{i}^{i=N\,Cells} \text{Cell Pore Volumes } (\text{where } t_i < t) \text{ or } (\text{where } \tau_i < \tau) \tag{22}$$

Where t_i or τ_i denotes the arrival time for a particular cell and t or τ denotes the time at which the drainage volume is being calculated.

For illustrative purposes, the drainage volume for a heterogeneous reservoir (permeability variation shown in **Fig. 6(a)**) has been calculated by using the FMM(Xie et al. 2012). Assuming the reservoir and fluid properties and the well configuration shown, the FMM solution gave the areal arrival time map shown in **Fig. 6(b)**. The drainage volume at different times has been shown in **Fig. 6(c)** and the calculations were completed in a matter of seconds.

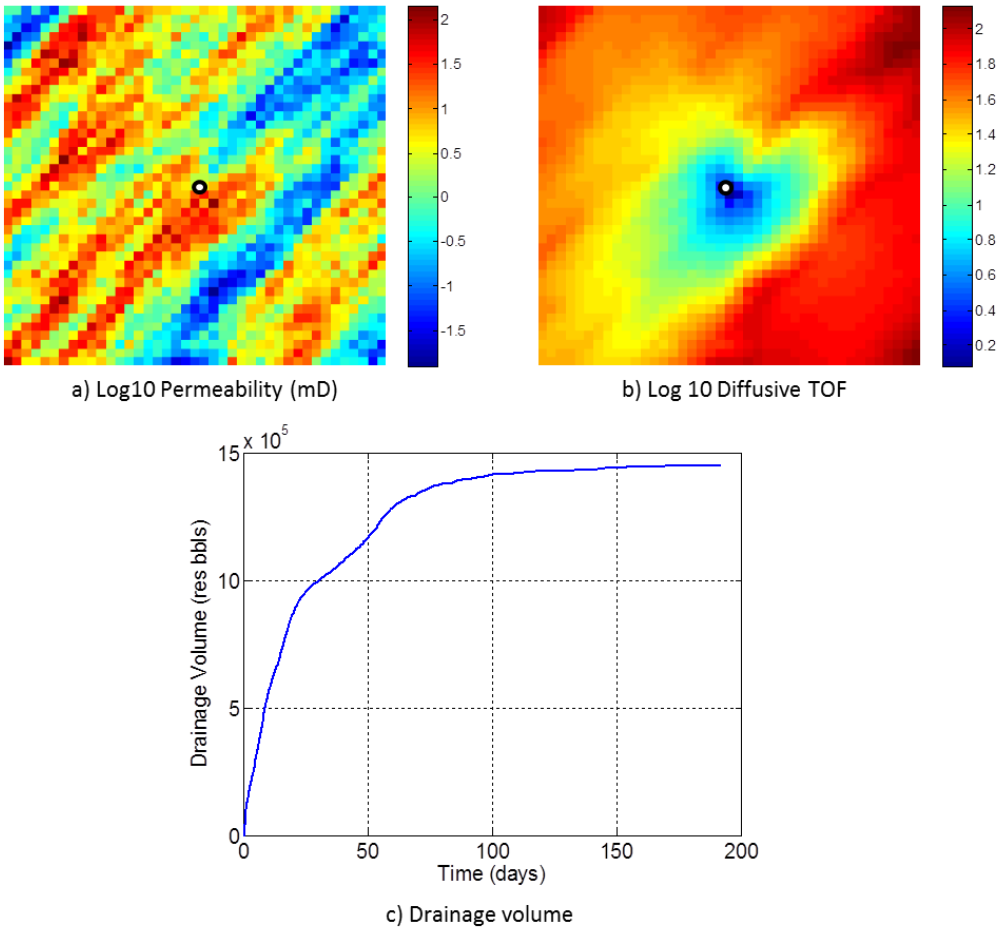

Fig. 6—Example to illustrate the drainage volume calculation. (a) permeability distribution (log scale), (b) time of flight (log scale), and (c) drainage volume variation with time

As explained above, the current FMM algorithm is based on a five point scheme, a very simple implementation (seven points in 3D) and with fixed cell dimensions Δx, Δy, Δz on all cells. The drainage volume can be efficiently estimated for any general reservoir system, with additional complexities like heterogeneity, single/multiple hydraulically fractured well geometry and also bounded or semi-bounded reservoir geometry (Datta-Gupta et al. 2011). This semi-analytical methodology can prove especially beneficial for unconventional reservoirs, such as tight gas and shale gas reservoirs, for predicting the

pressure front propagation and drainage volume variation during long transient times. Once the drainage volumes have been calculated, a geometric approximation as explained in **Chapter III** can be applied to estimate the pressure depletion behavior.

2.3.1 Calculation of actual time from the diffusive time of flight

For simplified cases, where the flow is linear, radial or spherical, the coefficient value for converting the diffusive time of flight to actual time, can be directly used from **Table 1**. But for a general reservoir system, the flow regime might vary with time. As an example, for a vertically fractured well in a homogeneous reservoir, the flow would initially be linear, followed by a transition phase and then pseudo-radial. In order to capture this flow regime variation and the change in corresponding coefficients, the relation between drainage volume (V_p) and diffusive time of flight (τ) can be used. These relations have first been explained for linear (**Fig. 7(a)**), radial (**Fig. 7(b)**) and spherical (**Fig. 7(c)**) flow and then its application for two general cases has been shown.

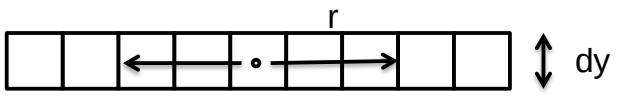

(a)

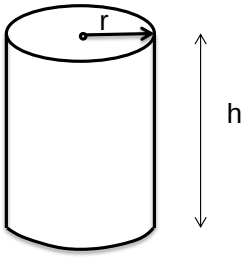

(b)

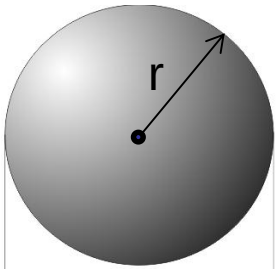

(c)

Fig. 7—Representation of the general flow types and the dimensions involved to estimate the drainage volume for (a) linear (b) radial and (c) spherical flow geometry

In a homogeneous reservoir with constant diffusivity (α) and linear, radial or spherical flow, the common relation between radial distance and diffusive time of flight is given by **Eq. (23)**:

$$r = \sqrt{\alpha \tau} \tag{23}$$

By the use of this relation, the pore volume (V_p), usually expressed in terms of radius, can now be expressed in terms of the diffusive time of flight (**Table 3**). It was observed that when these two parameters, V_p and τ are plotted on a log log scale, a distinct slope

can be obtained for linear, radial and spherical flows as shown in **Fig. 8 – 10**. This is the standard method for calculating a fractal dimension (Mandelbrot 1982). In our case, we obtain integer dimension. The coefficient for tau to time conversion is then simply expressed as twice the value of observed slope (**Table 3**). Thus, for a general reservoir system, the conversion coefficient can be obtained as a function of τ and then the actual time calculation can be generalized as **Eq. (24)**:

$$t = \left(\int \frac{1}{\sqrt{c_r}} d\tau \right)^2 \tag{24}$$

Table 3. Drainage volume for flow types and the corresponding log-log plot slope between pore volume and diffusive time of flight and the conversion coefficient

Flow Type	Vp	Vp = fn (τ)	Log Log Plot Slope	C_r
Linear	2 r dy dz	$2\sqrt{\alpha}\ \tau$ dy dz	1	2
Radial Cylindrical	$\pi\ r^2$ h	$\pi\ \alpha\ \tau^2$ h	2	4
Spherical	$4/3\ \pi\ r^3$	$4/3\ \pi\ \alpha^{1.5}\ \tau^3$	3	6

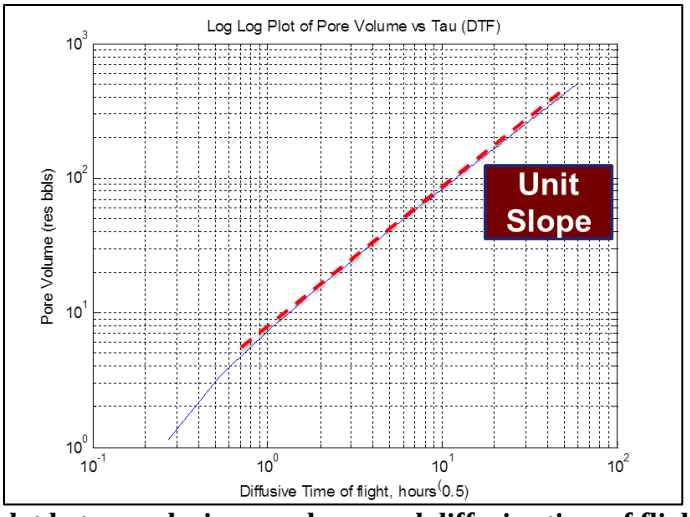

Fig. 8—Log log plot between drainage volume and diffusive time of flight for linear flow

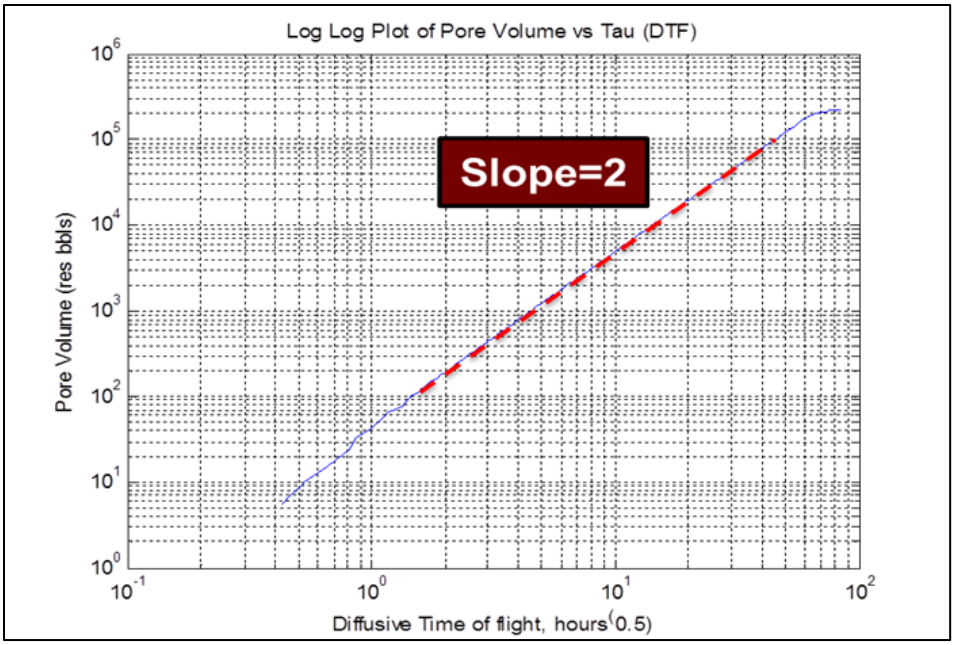

Fig. 9—Log log plot between drainage volume and diffusive time of flight for radial flow

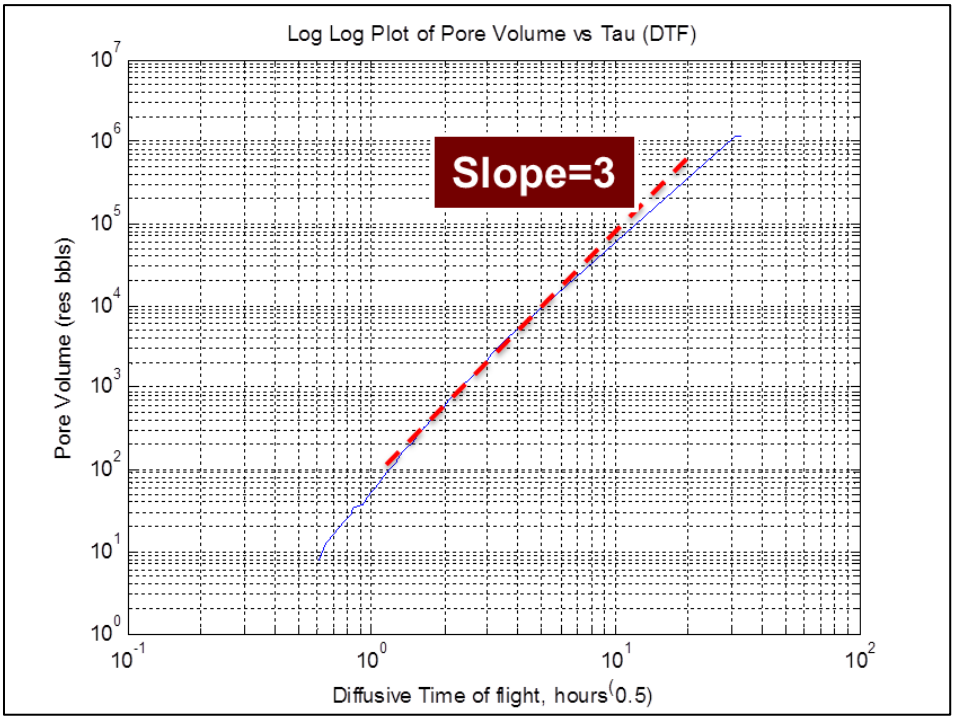

Fig. 10—Log log plot between drainage volume and diffusive time of flight for spherical flow

Applications

Well in a channel

For this case, the well is placed in a channel connected to another larger channel as shown in **Fig. 11**. The flow should initially be radial, transitioning to linear and then semi-radial flow. So according to the above derived relations, the slope observed in the V_p v/s τ log log plot should be 2, 1 and 2 respectively. And as we can see in **Fig. 12**, showing the log lop plot, these slopes can be distinctly observed. Thus this shows that this relation is well expressed for a general homogeneous case.

The duration of the flow regimes depends on the length and width of the channel. If the first channel is of comparable length to the connected channel, the results for time by using variable coefficients would be between the results obtained by using a single coefficient of 2 or 4, as shown in **Fig. 13**. But as the length of the channel increases, let's say about four times than the connected channel, the duration of linear flow increases (**Fig. 14**) and the results for time by using variable coefficients moves closer to that obtained by using a single coefficient of 2 (**Fig. 15**).

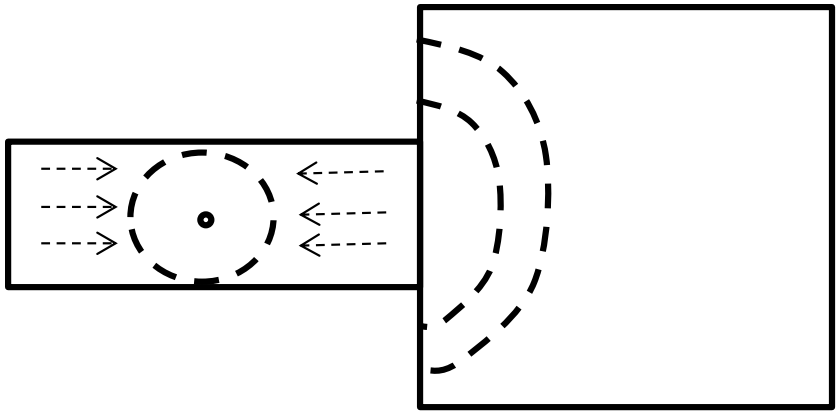

Fig. 11—Example for flow regimes of a well located in a channel

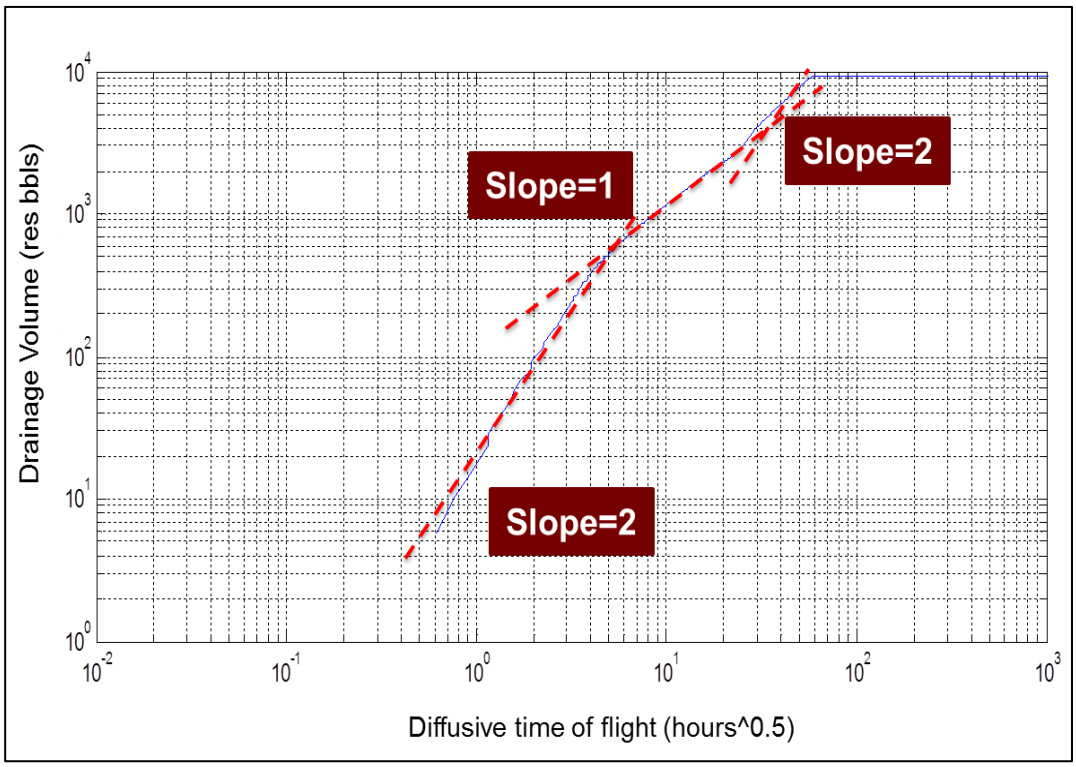

Fig. 12—Log log plot between drainage volume and diffusive time of flight for a well in a channel

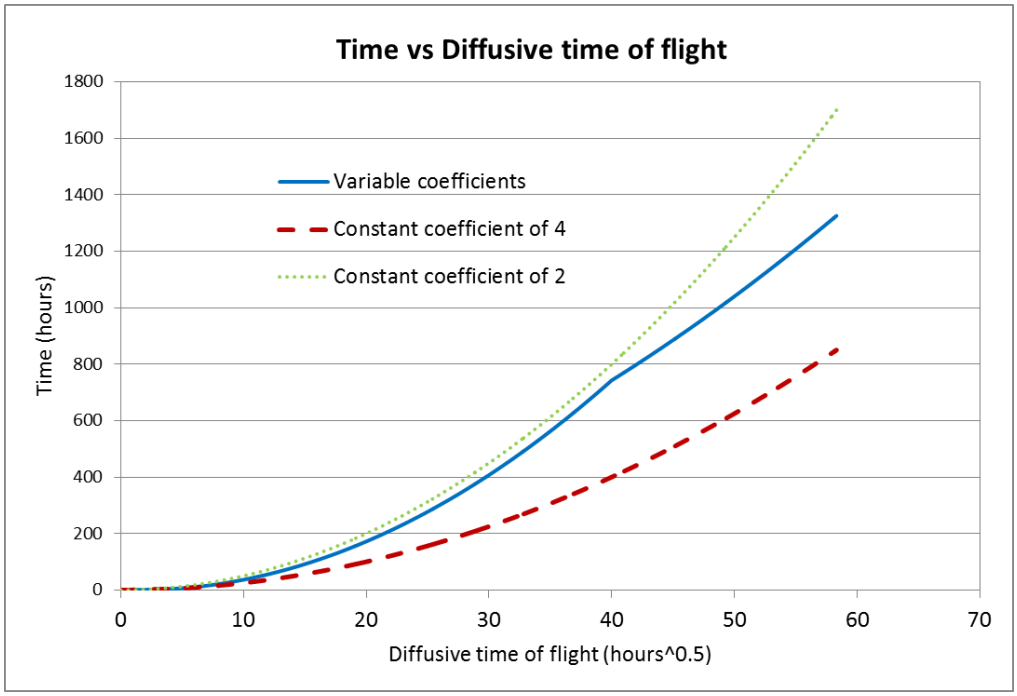

Fig. 13—Actual time v/s diffusive time of flight for a smaller channel to show the deviation by using a single coefficient of 2 or 4

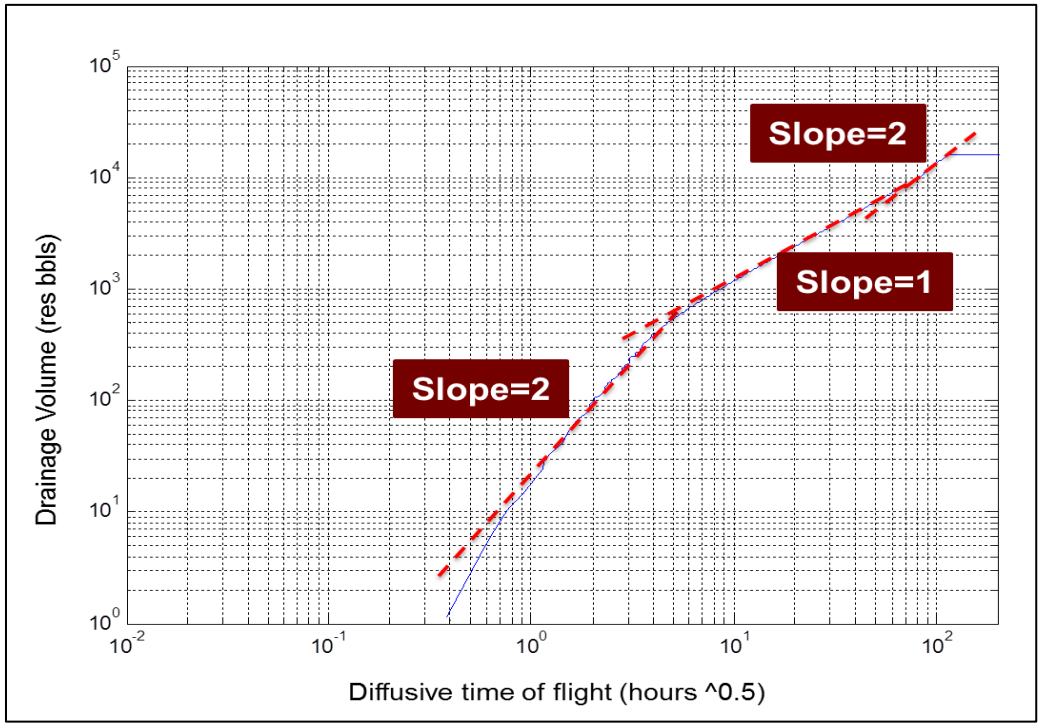

Fig. 14—The variation in the duration of the flow regimes if the channel length increases

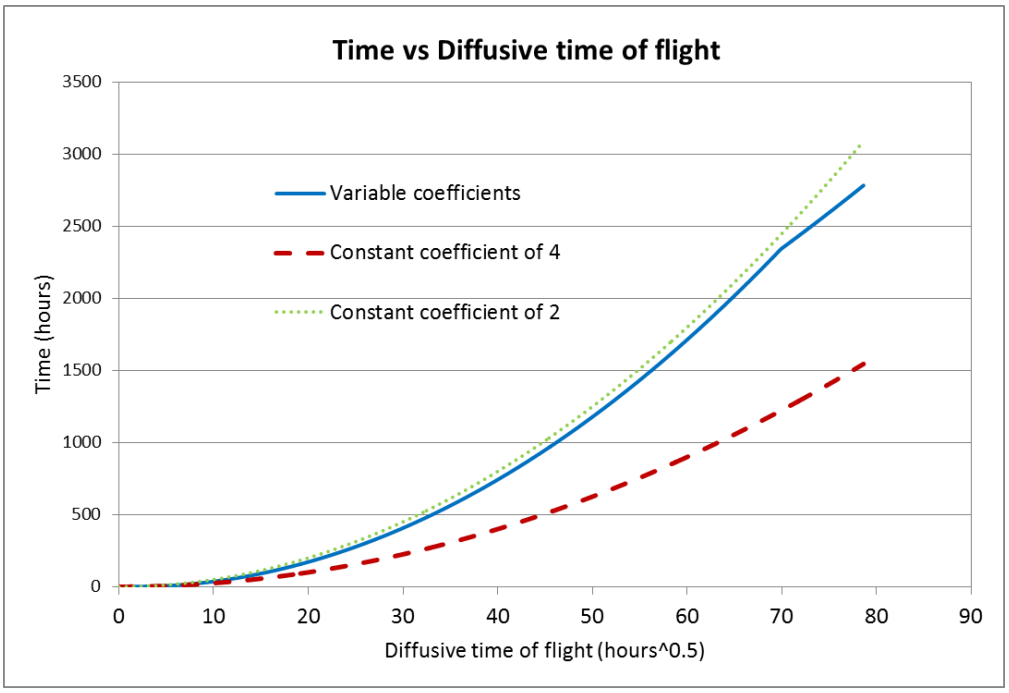

Fig. 15—Actual time v/s diffusive time of flight for a longer channel to show the deviation by using a constant coefficient of 4

Well in the center of a thick layer

For this case of a well placed in the center of a thick layer (as in **Fig. 16**), the flow should initially be spherical, until it reaches the top or bottom of the reservoir and then pseudo-radial assuming that the other boundaries of the layer are far away. So accordingly the slope observed in the V_p v/s τ log log plot should be 3 and then 2, which can also be clearly seen in the **Fig. 17**. Thus this again shows that this relation is well expressed for any general homogeneous case. The diffusive time of flight can be converted into actual time by using variable coefficients, which is different from using a single coefficient, as shown in **Fig. 18**.

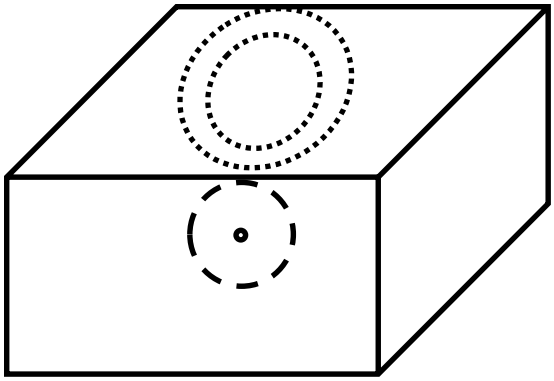

Fig. 16—Example for flow regimes of a well located in the center of a layer

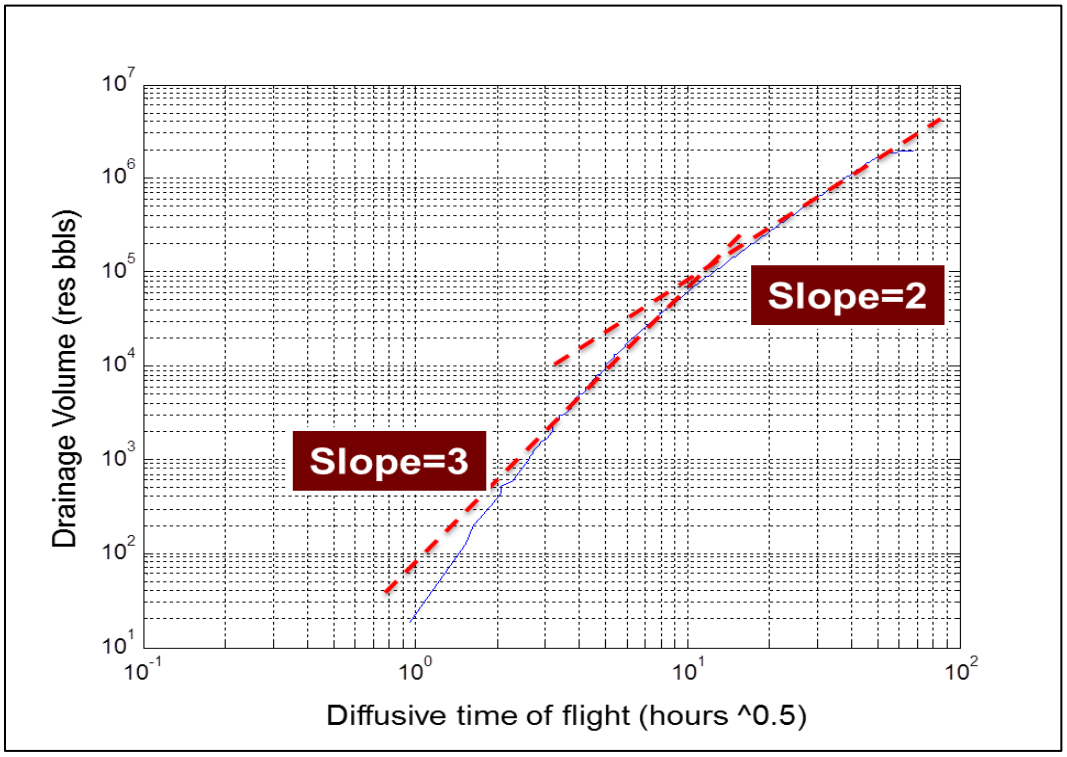

Fig. 17—Log log plot between drainage volume and diffusive time of flight for a well located in the center of a layer

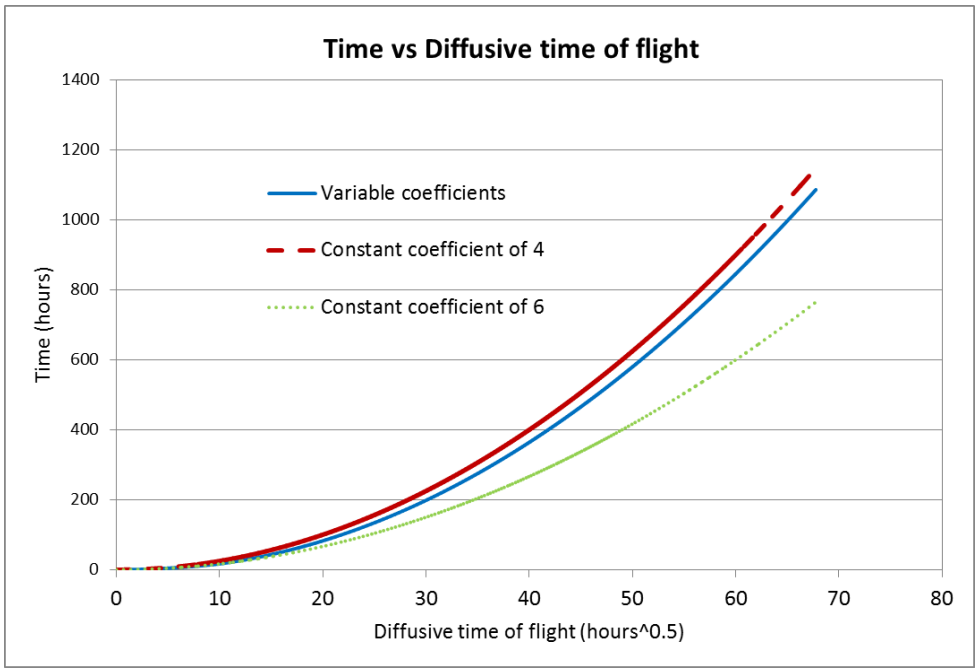

Fig. 18—Actual time v/s diffusive time of flight for a well in a layer

Based on these applications to homogeneous reservoirs, we have established a distinct relation between drained volume and the diffusive time of flight to obtain the conversion coefficient and hence the actual time. The same methodology can be extended to heterogeneous reservoirs. Depending upon the connectivity of the pressure propagation, the slope values need not be integer, e.g., unconventional reservoirs.

CHAPTER III

GEOMETRIC APPROXIMATION FOR PRESSURE AND RATE SOLUTION

Chapter III discusses the prediction of pressure and production behavior of a generalized reservoir system by application of a geometric approximation (Xie et al. 2012). This approximation utilizes the drainage volumes estimated by the Fast Marching Method approach as explained in the previous **Section 2.3.3**. For a well producing at constant rates, this solution determines the pressure depletion at any location in the reservoir and at any given time. Also, this approximation can be extended to a well producing with constant bottomhole pressure, for obtaining the production rate solution.

3.1 Geometric pressure solution

This geometric approximation utilizes the estimated drainage volume for any transient time and applies the pseudo steady state material balance concepts for predicting the reservoir pressure depletion. This approach can be explained by going back to **Eq. (2) & (3)**, written specifically for radially symmetric flow as **Eq. (25) & (26)**:

$$A(r)\phi c_t \frac{\partial P}{\partial t} = \frac{\partial Q}{\partial r} \tag{25}$$

$$Q = \frac{kA(r)}{\mu}\frac{\partial P}{\partial r} \tag{26}$$

where,

$A = 2\pi rh$, $r = \sqrt{x^2 + y^2}$ for cylindrical radial flow,

$A = 4\pi r^2$, $r = \sqrt{x^2 + y^2 + z^2}$ for spherical radial flow, and

A is a constant, $r = |x|$ for linear flow.

The sign convention we are using has Q_w for a producer, and Q is the inwardly directed flux. The pore volume for such cases can be expressed as **Eq. (27)**:

$$V_p(r) = \phi \int_0^r A dr \tag{27}$$

When **Eq. (25)** is expressed in terms of the pore volume, it becomes the material balance equation as **Eq. (28)**:

$$c_t \frac{\partial P}{\partial t} = \frac{\partial Q}{\partial V_p} \tag{28}$$

Now, this equation can be utilized to obtain a geometric pressure solution by making the following assumptions:

(a) The drainage volume acts as a moving no flow boundary and the Darcy flux is negligible outside the pressure front

(b) Within the drainage volume, the pressure is well approximated by a steady state solution.

(c) The well is producing at a constant rate, Q_w.

When these conditions are applied to the material balance **Eq. (28)**, it simplifies to the following **Eq. (29)**, which can be used to estimate the pressure drop at any point anytime.

$$\frac{\partial P}{\partial t} \cong \frac{\partial \overline{P}}{\partial t} = -\frac{1}{c_t}\frac{Q_w}{V_p(r(t))} \tag{29}$$

This equation is well known in the industry for the pseudo steady state average pressure drop calculations but our approach has generalized it for transient flow, by applying this concept to the moving drainage boundary, $V_p(r(t))$. This equation can also be used to calculate the pressure derivative (**Eq. (30)**) which can be used in the interpretation of drainage volume, as a function of time. As can be seen in the equation, once the drainage volume becomes constant, a typical unit slope would be observed in the log log plot. Other flow regimes arise during transient flow.

$$\Delta P' = -t\frac{\partial P}{\partial t} \cong -t\frac{\partial \overline{P}}{\partial t} = \frac{1}{c_t}\frac{Q_w t}{V_p(r(t))} \tag{30}$$

Once the derivative is known, it can be integrated to obtain the actual pressure drop at any location**,** starting from the time at which the approximate zero pressure contour passes over a location up to the time of interest. The approximate zero pressure contour is not necessarily at the depth of investigation and can be determined by using an approach developed by Nordbotten et al. (2004) as further illustrated in **Section 3.1.1**. Agarwal (2010) recently introduced a similar approach to determine the variable drainage volume but it requires a known pressure response and can be applied only for radial cylindrical systems. Therefore, our work is the first where this concept has been

generalized for heterogeneous reservoirs and both the drainage volumes and pressure response can be estimated.

To illustrate the pressure derivative and pressure calculation, let us consider an example of infinite acting cylindrical radial flow where the depth of investigation is given by, $r = \sqrt{4kt/\phi\mu c_t}$. By using this relation to calculate drainage volume and then substituting it to obtain the well test derivative, we get $\Delta P' = \frac{\mu Q_w}{4\pi kh}$ which is the well-known result. The approximation of the pressure drop as a natural logarithm is obtained by integrating Equation 30. It is not necessary to develop the full Ei solution as an intermediate step to obtain these results, as is usually done. In addition, there is no requirement for a radially symmetric solution, once we apply the drainage volume concept to heterogeneous systems, as is shown in **Fig. 19 & 20** for the same permeability distribution in **Fig. 6**.

While applying the asymptotic limit of the pressure equation to heterogeneous reservoir, we have made an underlying assumption that the heterogeneity contrast between adjacent reservoir cells is not very high. This assumption is required so that the pressure drop at any point is primarily due to the first arrival pressure waves (direct or transmitted) and the pressure drop due to pressure waves reflected from media boundaries is minimal. In order to study this limitation and to make sure that the approximation is reasonable, the magnitudes for transmitted and reflected waves were calculated as explained in detail in **Section 3.1.2**.

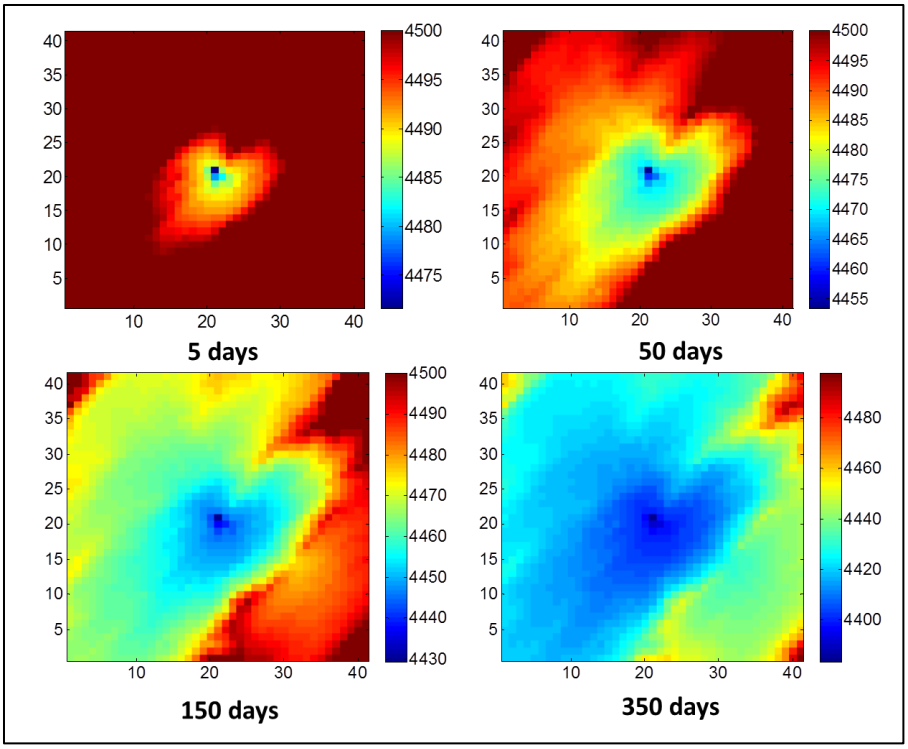

Fig. 19—Pressure distribution obtained by applying the geometric approximation, at the end of 5 days, 50 days, 150 days and 350 days

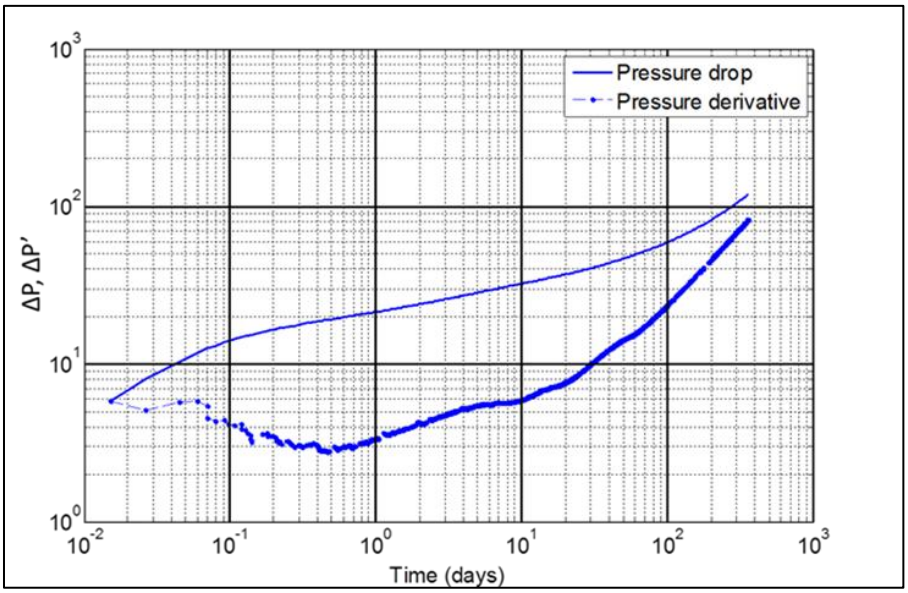

Fig. 20—Pressure derivative obtained for the example by applying the geometric approximation

3.1.1 Asymptotic limits for the pressure and rate solution

As mentioned in the previous **Section 2.1**, we are using the definition of the depth of investigation as the depth where the pressure derivative is a maximum. This depth can give us a good estimate of the drainage volume but it does not imply that the pressure drop and flux at this depth exactly vanish. Therefore, it is important to determine the asymptotic solution for the zero pressure contour for accurate integration of the pressure derivative (as obtained by the geometric approximation) to determine the pressure drop in the drained volume.

To obtain these solutions, we have utilized a similar approach as Nordbotten et al. (2004) where they expanded the well function in a radial system (exponential integral) by using an infinite series approximation. They developed this solution to determine the leakage volume in a water reservoir but these concepts can easily be extended to our reservoir system. The well function for a producer in a radial system is given by **Eq. (31)** (Lee 1982):

$$\Delta P(r,t) = \frac{Q_w \mu}{4\pi k h} Ei\left(\frac{r^2}{4T}\right) \tag{31}$$

The Ei function is the well-known exponential integral function and it can be approximated by the infinite series approximation in **Eq. (32):**

$$Ei(-x) = -0.5772 - \ln(x) + x - \frac{x^2}{2.2!} + \frac{x^3}{3.3!} - \frac{x^4}{4.4!} + \frac{x^5}{5.5!} - \frac{x^6}{6.6!} + .. \tag{32}$$

Substituting this equation back in **Eq. 31**, the pressure drop solution can now be expressed as a series of terms. In order to obtain the asymptotic pressure solution, the term $\Delta P(r,t)$ should be equated to zero and different solutions for this can be obtained depending on the numbers of terms used from the infinite series expansion.

This asymptotic solution provides the location of the expanding outer boundary which would act as a cut-off, beyond which the pressure response can be considered negligible. **Fig. 21** shows various solutions for the pressure drop value by using different terms in the expansion and the corresponding location of the outer boundary.

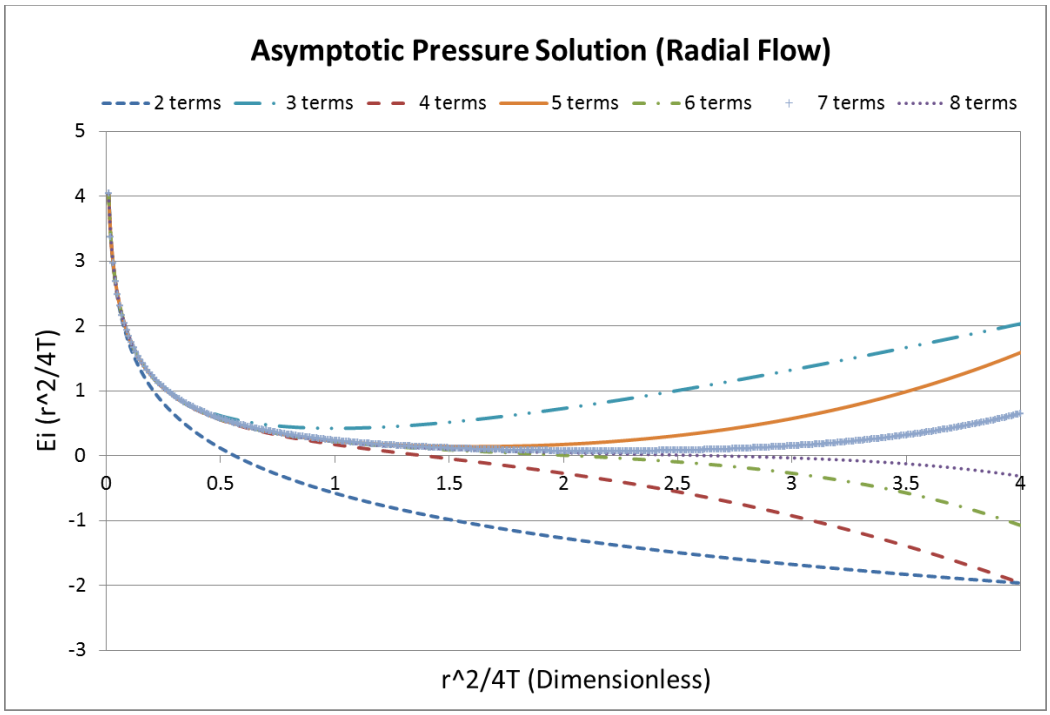

Fig. 21—Asymptotic pressure solution for radial flow by using different terms in the infinite series expansion

However, only even terms give solutions for outer boundary for a radial system. As seen in **Fig. 21**, the radius is always a function of the square root of time. The two term logarithmic solution corresponds to the steady state solution of the partial differential equation defined on a finite domain. While for higher number of terms, the solution represents a truncated transient solution. For linear and spherical flow, the zero pressure boundaries by using a two-term expansion have been shown in **Table 4**. From the results, it was observed that for all these cases, the zero pressure drop boundary lies within the radius of investigation. Therefore, the pressure drop calculations should use this reduced boundary for more accurate results when integrating the pressure derivatives.

Analogous to the asymptotic pressure solutions, we can also obtain the asymptotic flux solutions using the same approach. These asymptotic flux solutions can be used for accurate integration over boundaries in the transient rate solutions, as explained in the coming **Section 3.2**. Let us illustrate the solution for a radial system first, where the flux function at any distance in the reservoir can be given by **Eq. (33)**:

$$Q(r,T) = Q_w Exp\left(-\frac{r^2}{4T}\right) \tag{33}$$

'Exp' is the exponential function which can be expanded with an infinite series approximation as **Eq. (34)**:

$$Exp(-x) = 1 - x + \frac{x^2}{2!} - \frac{x^3}{3!} + \frac{x^4}{4!} - \frac{x^5}{5!} + \frac{x^6}{6!} + .. \tag{34}$$

Again by using different number of terms in the expression and equating Q(r,T)=0, the asymptotic flux solutions can be obtained. **Fig. 22** shows the flux values by using different terms in the expansion and also, the location of the corresponding outer boundary.

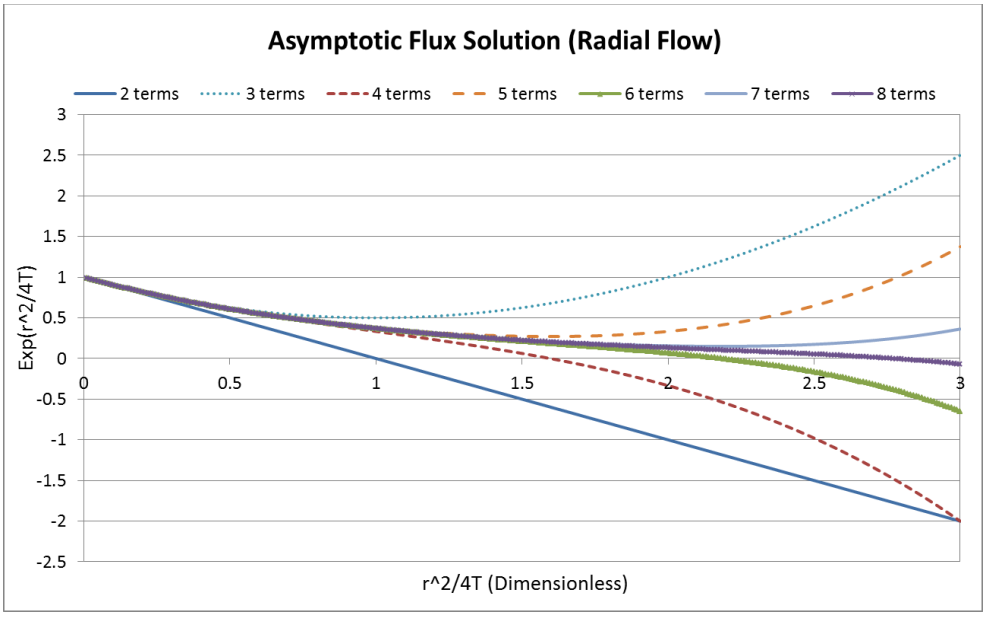

Fig. 22—Asymptotic flux solution for radial case by using different terms in the exponential function expansion

The solutions for linear, radial and spherical flow by using a two-term expansion have been shown in **Table 4**. It can be seen that for a radial case, the zero flux boundary is identical to the radius of investigation. For linear, it lies outside the radius of investigation while for spherical, it lies inside the radius of investigation.

Table 4. Location of the zero isobar radius, zero flux radius and the radius of investigation for different flow types

Flow Type	Zero Isobar Radius	Zero Flux Radius	Radius of Investigation
Linear	$r = \frac{2}{\sqrt{\pi}}\sqrt{T}$	$r = \sqrt{\pi T}$	$r = \sqrt{2T}$
Radial	$r = e^{-\frac{\gamma}{2}}\sqrt{4T}$	$r = \sqrt{4T}$	$r = \sqrt{4T}$
Spherical	$r = \sqrt{\pi T}$	$r = \sqrt{(16\pi)^{1/3}T}$	$r = \sqrt{6T}$

3.1.2 First pressure wave arrival approximation

To understand this concept, we need to understand that similar to optic rays and electro-magnetic waves, the pressure waves also is reflected and transmitted on interaction with a media boundary (Oliver 1994) . This has been explained in the schematic diagram (**Fig. 23**) where two media are considered with properties (k,ϕ) and (k', ϕ') and the source well producing at rate Q_w is located in the first medium. Once the pressure waves start propagating from the source (point A) in medium 1, it reaches the media boundary at different points and angles at different times. As an example, let us consider the wave incident at point C on the boundary, at an angle θ_i with the normal and at distance τ from point A. Now, the pressure drop at any point (B) in the first medium located at an equal distance τ from point A, can be calculated by adding up the pressure drop due to the direct wave from the source at A and the pressure drop due to the reflected wave from the media boundary (point C) at an angle (θ_r) arriving at a later time. Similarly, for any point in medium 2 (point D) also located at distance τ from point C, the pressure drop

would be due to the transmitted wave across the boundary, at an angle θ_t from the normal.

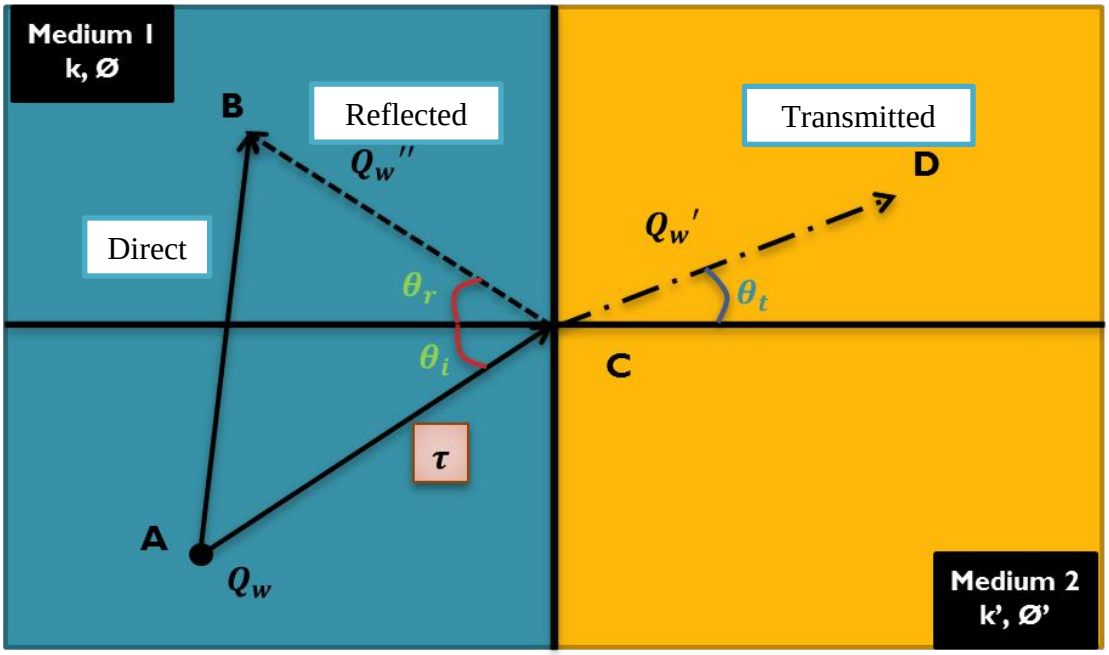

Fig. 23—Schematic to explain the pressure wave interaction at the media boundary

Keeping in mind this wave behavior, we are considering the following underlying assumptions while applying the geometric approximation in case of heterogeneous reservoirs and reservoirs with boundaries:

- The pressure drop at any point is only due to the first direct pressure wave arrival at that point and the pressure drop caused by the reflected wave is negligible
- The magnitude of the transmitted wave across the media boundary is close to the direct source wave

Therefore, in order to apply the first arrival approximation correctly, it is important to understand the magnitude of the direct, reflected and the transmitted waves coming from a source Q_w. Let us assume that the magnitude of the reflected wave is Q_w'' and that of the transmitted wave is Q_w'. Now, for estimating these magnitudes, we have considered the following concepts:

1. The normal component of flux at the boundary is equal, which gives **Eq. (35)**

$$\sqrt{\frac{\phi}{k}}\left(Q_w - Q_w''\right)\cos\theta_i = \sqrt{\frac{\phi'}{k'}}Q_w'\cos\theta_t \tag{35}$$

2. Pressure drop at the incident point should be same in both the media, which gives **Eq. (36)**

$$\frac{Q_w + Q_w''}{k} = \frac{Q_w'}{k'} \tag{36}$$

3. The pressure wave would follow the shortest path to reach to any point across the boundary, which gives **Eq. (37)**

$$\sqrt{\frac{\phi}{k}}\sin\theta_i = \sqrt{\frac{\phi'}{k'}}\sin\theta_t \tag{37}$$

By using **Eq. (35)-(37)** and substituting the variables, the transmitted wave and the reflected wave magnitudes were determined as **Eq. (38)** and **Eq. (39)** respectively:

$$Q_w' = \frac{2Q_w}{\left(\frac{k}{k'} + \sqrt{\left(\frac{\phi' k}{\phi k'} - 1\right)\sec^2\theta_i + 1}\right)} \tag{38}$$

$$Q_w^{''} = Q_w \left(\frac{2}{\left(1 + \frac{k'}{k}\sqrt{\left(\frac{\phi' k}{\phi k'} - 1\right)\sec^2\theta_i + 1}\right)} - 1 \right) \tag{39}$$

The other observation was that the angle at which the pressure waves get reflected is same as the incident angle. While, the magnitude of the angle at which the waves get transmitted in the other medium follows the relation in **Eq. (40)**:

$$\theta_t = \sin^{-1}\left(\sqrt{\frac{\phi k'}{\phi' k}}\sin(\theta_i)\right) \tag{40}$$

Based on these derivations, a sensitivity analysis was done for the parameters like permeability contrast, porosity contrast and incident angle. The following conclusions were drawn from the results:

- The higher the permeability and porosity contrast, the larger is the error in considering the transmitted wave magnitude to be the same as the direct wave. Also the angle at which the waves get transmitted becomes lower with an increase in permeability contrast. The impact of varying permeability contrast on the transmitted wave ratio and the reflected wave ratio has been shown in **Fig. 24**. The assumed incident angle is 30 degrees. As seen in the figure, the response of transmitted wave ratio is quite close to the reciprocal of the perm contrast ratio. In **Fig. 25**, the variation of the transmitted angle has been shown for different permeability contrast ratios.

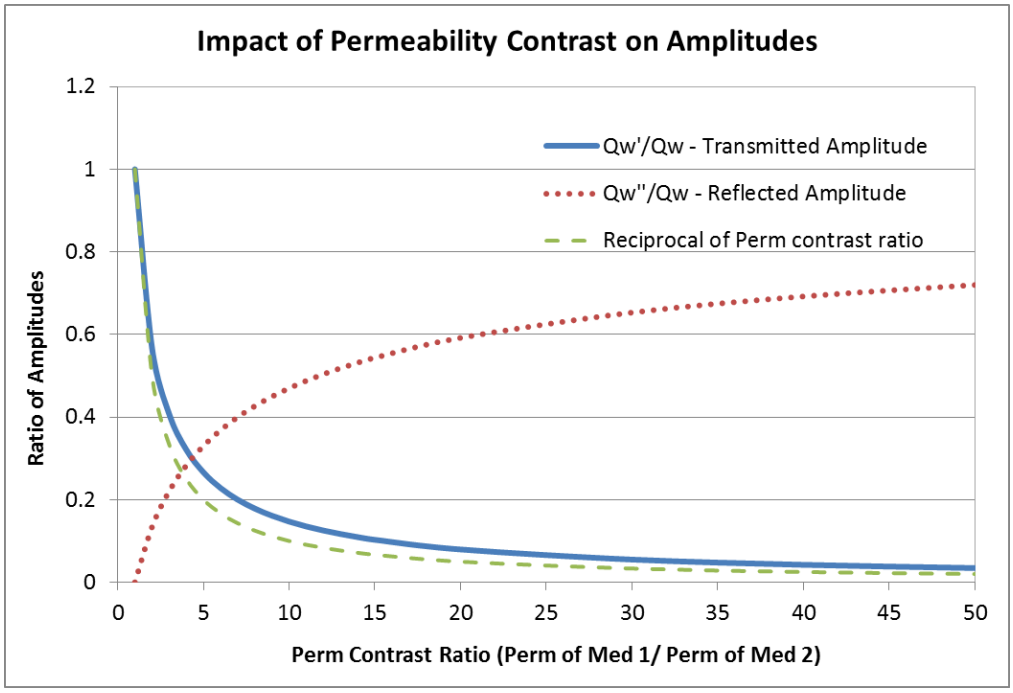

Fig. 24—Impact of varying permeability contrasts on the transmitted and the reflected wave magnitudes

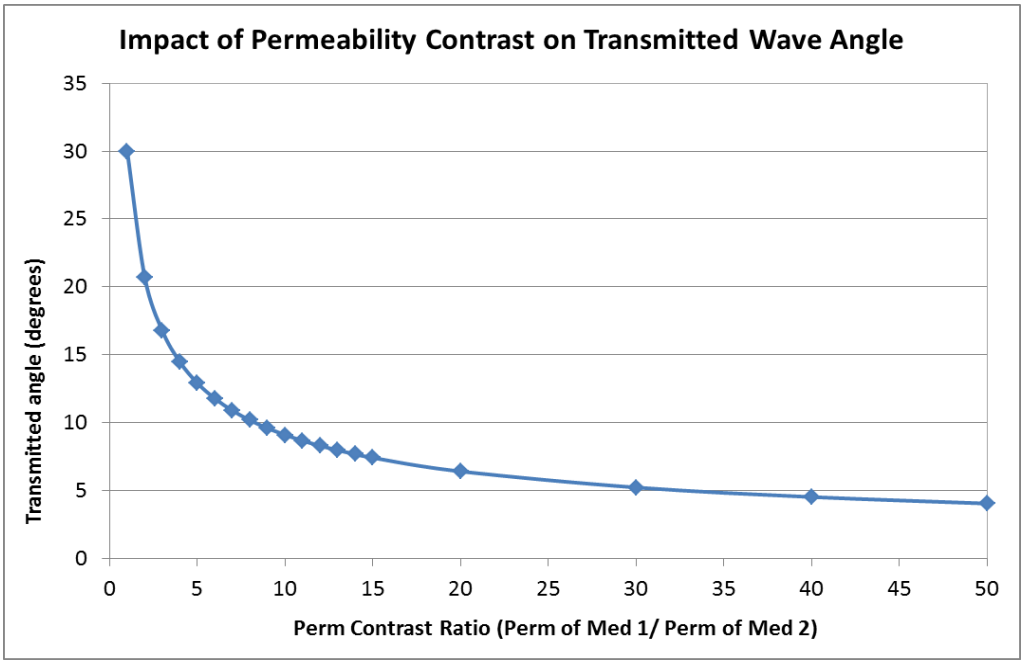

Fig. 25—Impact of permeability contrast on the transmitted angle

- If the permeability contrast is same as the porosity contrast, the transmitted angle is always same as the incident angle. But the transmitted wave and the reflected wave magnitude vary based on the contrast ratio as shown in **Fig. 26**.

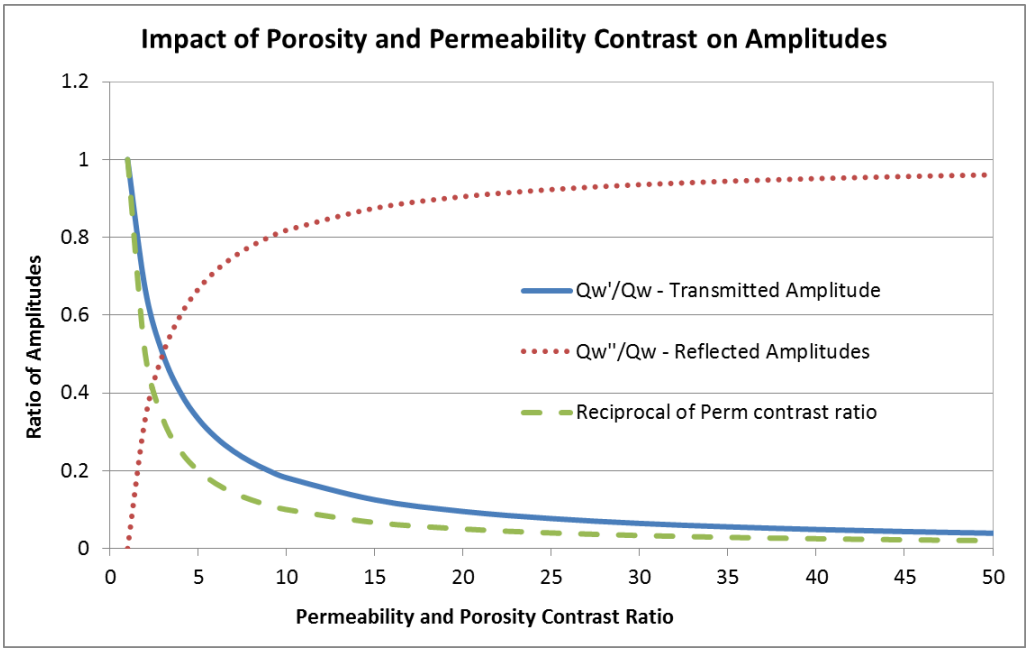

Fig. 26—Impact of porosity and permeability impact on transmitted and reflected wave magnitudes

- For a given permeability contrast, assuming same porosities, there is a critical incident angle above which the transmitted angle becomes 90 degrees, similar to the total internal reflection obtained in ray optic theory. This happens when the pressure wave is moving from lower to higher permeability media, as shown in **Fig. 27,** for a permeability ratio of 0.5. If the permeability contrast becomes very high, the path of shortest time would require minimum distance to be covered in the slow medium and the maximum distance in the fast one, as seen by the red line in **Fig. 28**. As an

example, the critical incident angle for a contrast ratio of 0.001 is 1.8 degrees, as seen in **Fig. 29**. In contrast, when the pressure wave is travelling from higher to lower permeability media, the reflected amplitude becomes zero beyond a critical angle and only transmitted amplitude can be obtained, as shown in **Fig. 30.** When this contrast becomes high, the path of shortest time would require maximum distance in the fast medium and minimum in the slow one, as shown by the green line in **Fig. 28**. As an example, the transmitted angle for the opposite contrast ratio of 1000 has been shown in **Fig. 31**, which shows the exact opposite path of the ratio of 0.001.

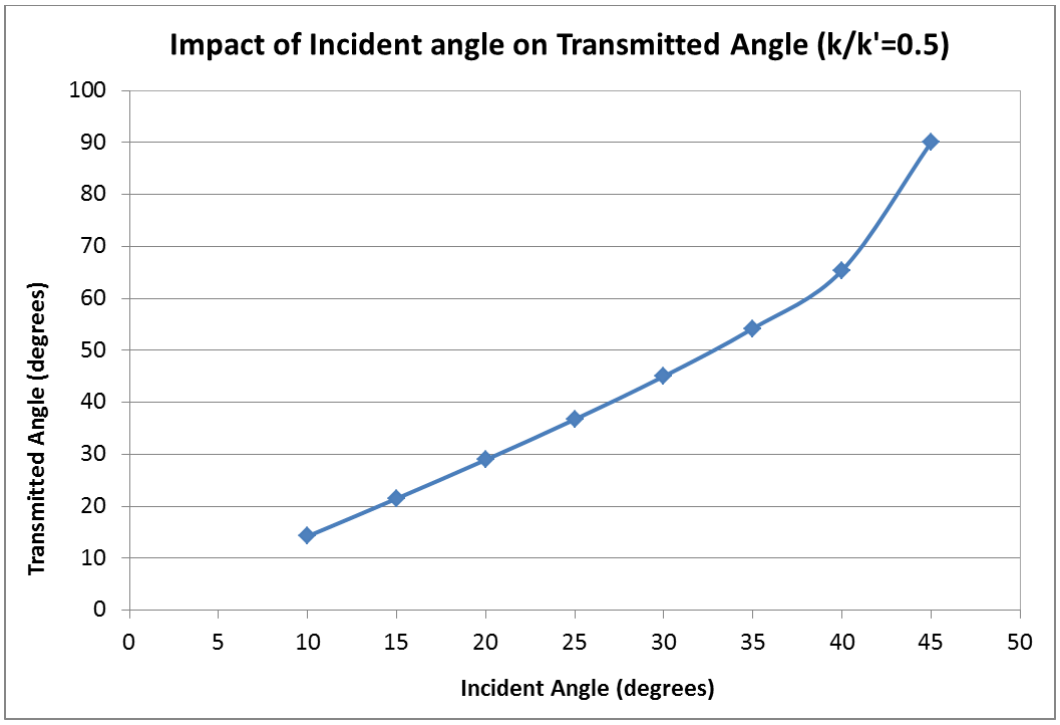

Fig. 27—Impact of incident angle on the transmitted angle for permeability ratio of 0.5 and zero porosity contrast

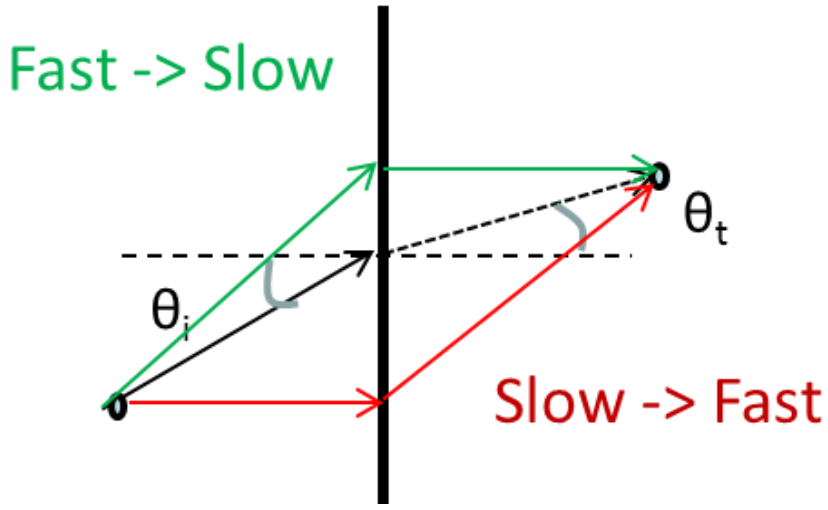

Fig. 28—Critical angles dependent on the extreme permeability contrasts

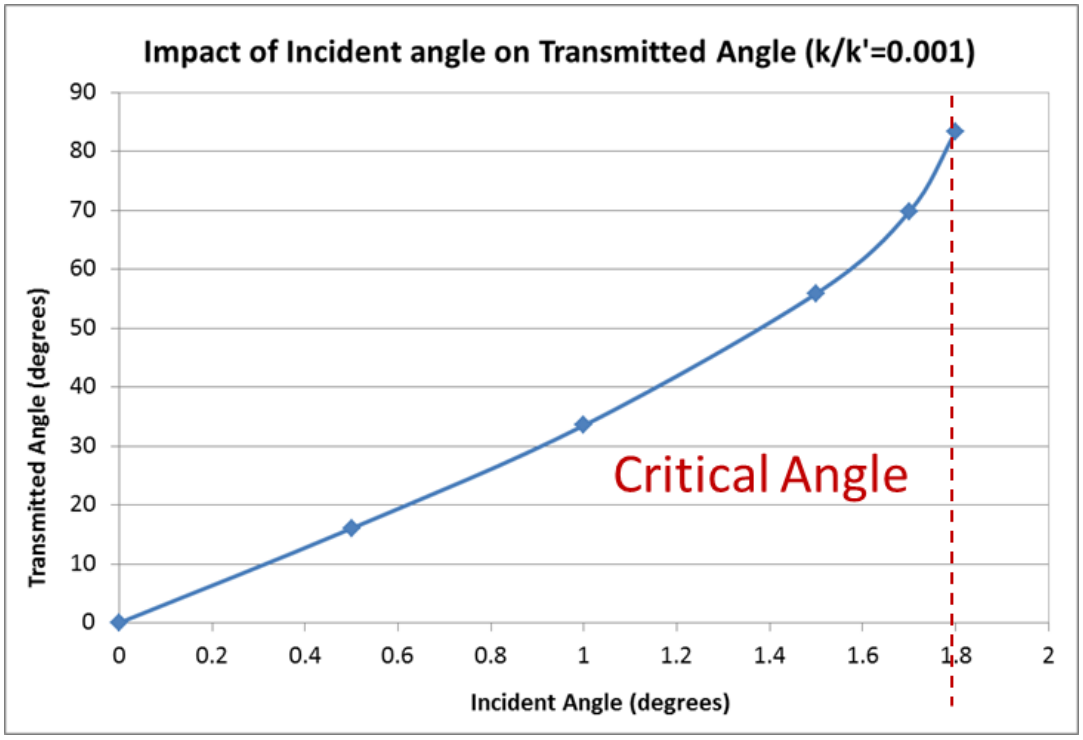

Fig. 29—Critical angle for a permeability contrast of 0.001

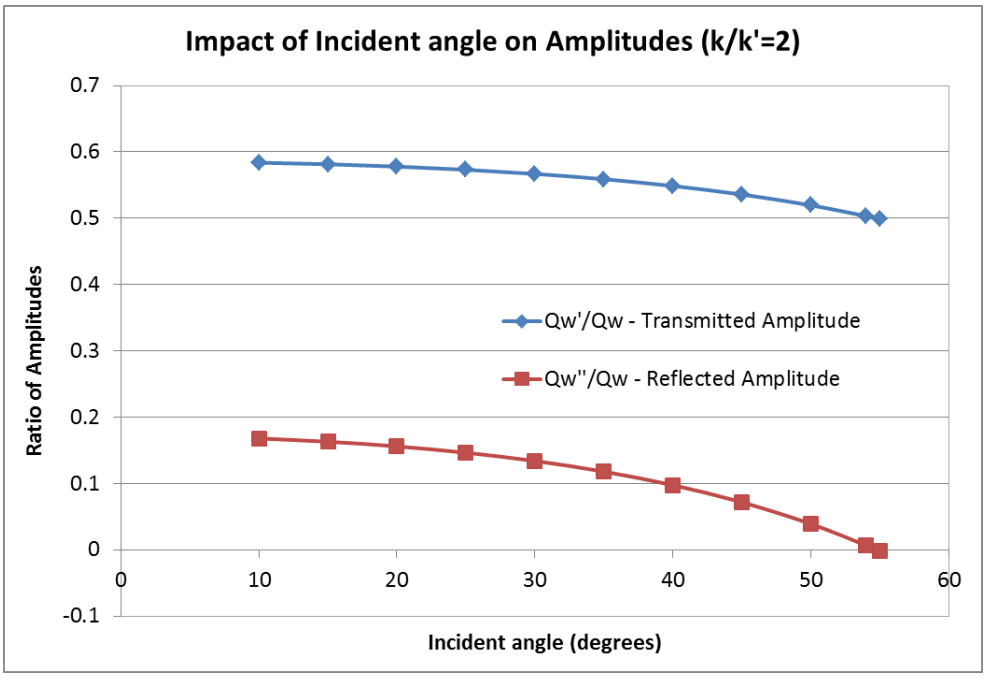

Fig. 30—Impact of incident angle on the amplitudes for permeability ratio of 2 and zero porosity contrast

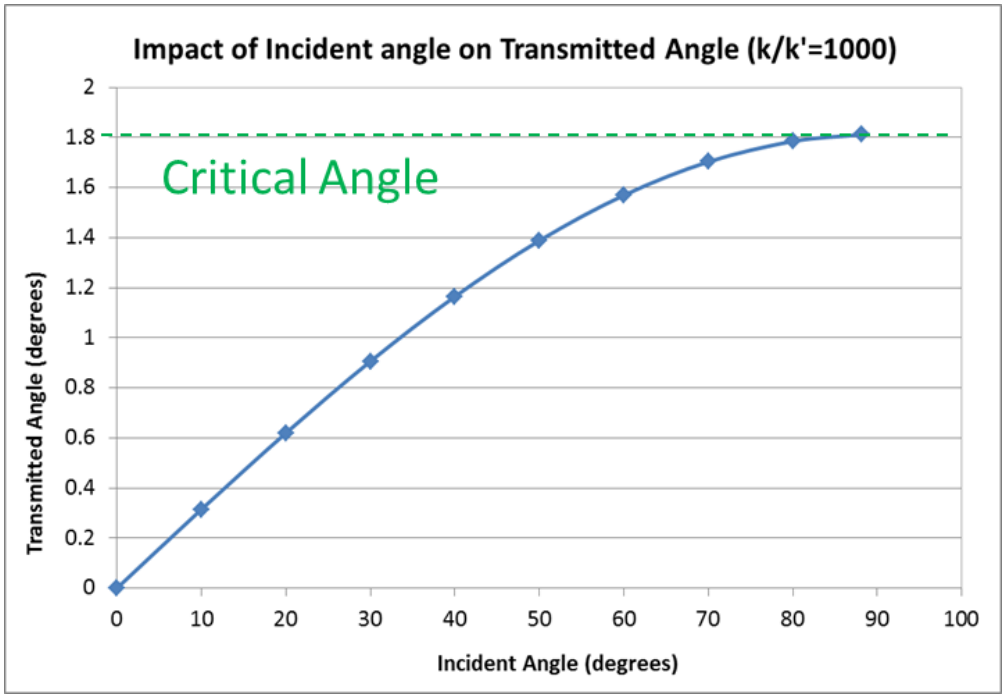

Fig. 31—Magnitude of the transmitted angles for a high permeability contrast ratio of 1000

Thus our geometric pressure approximation for heterogeneous reservoirs should be carefully used. The intent is not to compensate for these errors, but we should be aware of the limitations during specific applications.

3.2 Rate solution using geometric approximation

In the previous sections, all the derived solutions have been based on the assumption that the production rate of the well is constant. But the most common observation in fields is that the well produces with variable production rates. For production data analysis, most of the analytical solutions have been based on the pseudo steady state concepts and thus are not applicable for transient phases, predominant in unconventional reservoirs.

A transient rate solution for a radial well in an infinite acting reservoir has been provided by Fetkovich (1980). Based on this, the well-known Fetkovich type curves were generated for different reservoir properties, also combining the empirical Arp's solution for the pseudo steady state. Their biggest application is to estimate the basic reservoir properties by taking both the production data and bottomhole pressure data as input. Another commonly used plot for production data analysis introduces the term 'material balance time' but this also requires the cumulative production and rate data to back calculate the reservoir properties.

To obtain the transient rate solution for homogeneous cases, Laplace transforms have generally been applied (Lee 1982) but they cannot be extended to heterogeneous

reservoirs. Therefore, an attempt to generalize the transient analytical solution has been made in this work. To explain this concept, we will require the Darcy's Law (**Eq. (3)**) and **Eq. (27)** to estimate the drainage volume up to a zero flux radius. To obtain the solution, we also need to make the following assumptions:

- The well is producing with constant bottomhole pressure, P_{wf} and a slowly varying rate, Q_w at any time t.
- The reservoir outside the zero flux radius (r_{out}) is at initial conditions, with initial pressure P_i.
- The pseudo steady state solution is applicable within the drainage volume at any time ($V_p(r(t))$ such that the rate at any given radius with drainage volume, $V_p(r)$ can be calculated as in **Eq. (41)**.

$$Q(r) \cong Q_w\left(1-\frac{V_p(r)}{V_p(r(t))}\right) \tag{41}$$

Now, if we substitute **Eq. (41)** in the Darcy's law we obtain **Eq. (42)**:

$$Q_w\left(1-\frac{V_p(r)}{V_p(r(t))}\right)=\frac{k(r)A(r)}{\mu}\frac{\partial P}{\partial r} \tag{42}$$

This equation can be converted to use $V_p(r)$ as the independent spatial variable. The term ∂r can be expressed in terms of $\partial V_p(r)$ as **Eq. (43)**:

$$\partial V_p(r)=\phi(r)A(r)\partial r \tag{43}$$

By using this equation and applying the pressure limits at the well and the zero flux boundary to utilize the known pressure difference, the flux solution can be derived as in **Eq. (44)**:

$$Q_w = \frac{\left(P_i - P_{wf}\right)}{\mu} \frac{1}{\int_{r_w}^{r_{out}} \left(\frac{1}{\phi(r)k(r)A(r)^2} \left(1 - \frac{V_p(r)}{V_p(r_{out}(t))} \right) \right) dV_p(r)} \tag{44}$$

To establish its validity, we will now reproduce the transient rate solution for a radial system (Fetkovich 1980). For a homogeneous radial case, the porosity and permeability would be constant and the relation between flow cross-sectional area and drainage volume can be given as **Eq. (45)**:

$$A(r)^2 = 4\pi h V_p(r) \tag{45}$$

This equation when substituted in **Eq. (44)**, it becomes **Eq. (46)**.

$$Q_w = \frac{k\left(P_i - P_{wf}\right)}{\mu} \frac{1}{\int_{r_w}^{r_{out}} \left(\frac{1}{4\pi h V_p(r)} \left(1 - \frac{V_p(r)}{V_p(r_{out}(t))} \right) \right) dV_p(r)} \tag{46}$$

On solving this equation, it takes the form in **Eq. (47)**.

$$Q_w = \frac{4\pi kh\left(P_i - P_{wf}\right)}{\mu} \frac{1}{\left[\ln\left(\frac{r_{out}^2 - r_w^2}{r_w^2} \right) - 1 + \frac{r_w^2}{r_{out}^2 - r_w^2} \right]} \tag{47}$$

For large values of outer radius ($r_{out} >> r_w$), obtained at larger times, the above solution can be approximated as **Eq. (48).**

$$Q_w = \frac{2\pi kh\left(P_i - P_{wf}\right)}{\mu} \frac{1}{\left[\ln\left(\frac{r_{out}}{r_w}\right) - 0.5\right]} \tag{48}$$

This equation is the flux solution for a radial well with a skin of zero, thus demonstrating the consistency of our generalized flux solution, with known homogeneous solutions.

Similarly, the general expression for the flux in a single vertically fractured well can also be obtained. The cross-sectional area for flow and the pore volume in a fractured well case (**Fig. 32)**, assuming a super-position of radius of investigation around each point on the fracture, can be specified by using **Eq. (49)** & **Eq. (50).**

$$A = 2\pi r_{out} h + 4x_f h \tag{49}$$

$$V_p = \phi\left(\pi r_{out}^2 h + 4x_f r_{out} h\right) \tag{50}$$

Now by substituting these equations in our generalized flux solution (**Eq. (44)**), we obtain the following solution for a single vertical fracture flow as in **Eq. (51)**.

$$Q_w = \frac{4\pi kh\left(P_i - P_{wf}\right)}{\mu} \frac{1}{\left(1 + \frac{4h\phi x_f^2}{\pi V_p\left(r_{out}(t)\right)}\right)\ln\left(\frac{\pi V_p\left(r_{out}\right) + 4h\phi x_f^2}{\pi V_p\left(r_w\right) + 4h\phi x_f^2}\right) - 1 + \frac{V_p\left(r_w\right)}{V_p\left(r_{out}\right)}} \tag{51}$$

This solution can also reproduce the solution for transient rate solution given by Song et al. (2011), thus demonstrating the consistency.

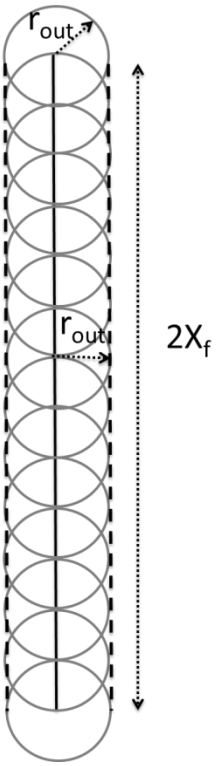

Fig. 32—Dimensions involved in a single vertically fractured well flow

The results obtained by this solution for a radial well and a single vertically fractured well have been shown in **Section 4.1.1 & 4.1.2**. They show very good agreement with the analytical and numerical solutions. We have not presented the results from this approximation for heterogeneous reservoirs, as that is still a work in progress. To utilize this solution, the FMM code would require additional calculations for estimating the flow cross-sectional area at all times, similar to the drainage volume calculations.

CHAPTER IV

RESULTS AND DISCUSSIONS

This chapter shows the application of our proposed methodology to several cases with homogeneous and heterogeneous property distributions (Xie et al. 2012). First we will describe several homogeneous cases with radial and single/multiple hydraulically fractured well geometries. With these cases, we will demonstrate the accuracy of our geometric pressure approximation and rate solution by replicating the results from analytical solutions in Sapphire (for pressure solution), Topaz (for rate solution) and numerical simulations conducted in CMG. In the results, we will show the drainage volume estimation, flow regime interpretation and the well bore pressure or rate variation by using our approach.

After this validation, we will discuss the application of this approach to unconventional reservoirs with heterogeneous property distributions, developed with multiple hydraulically fractured wells. We will provide flow visualization for the drainage volume variation and the flow regime interpretation for such cases.

4.1 Homogeneous cases

To study homogeneous cases, we have considered the following models most commonly used for studies:

1. Vertical radial well in an infinite acting reservoir

2. Single vertically fractured well in a rectangular reservoir

3. Horizontal well with multiple hydraulic fractures in a rectangular reservoir

Now we will give a description of the properties assumed for each of these case studies and the results obtained.

4.1.1 Vertical radial well in an infinite acting reservoir

This is a commonly used model for conventional reservoir studies. The analytical solution for transient radial flow in an infinite acting reservoir is well established. For comparison purpose, we have also obtained the results from numerical simulation using CMG. **Table 5** shows the reservoir and fluid properties assumed for this case.

Table 5. Properties for vertical radial well in an infinite acting reservoir

Property		Value	Unit
Reservoir	Porosity	0.25	fraction
	Permeability	1	md
	Thickness	10	ft
	Initial Pressure	4500	psi
Fluid	Viscosity	0.4	cp
	Oil FVF	1	
	Total compressibility	6.00E-06	1/psi
Well	Well radius	0.25	ft
	Well constant rate for pressure solution	10	bbl/day
	Well constant BHP for rate solution	1000	psi

For the case of an infinite acting radial reservoir, the drainage volume would vary with time with a straight line slope as shown in **Fig. 33**. This is because the drainage volume in radial reservoirs is proportional to the square of the radius which is proportional to actual time according to our definition of the radius of investigation. After the drainage volume calculation, the pressure drop and the pressure derivative were calculated for the well producing at a constant rate of 10 bopd, as shown in **Fig. 34**. This clearly shows the radial flow regime with a slope of zero in the pressure derivative plot.

The calculated well bottomhole pressure based on our approach was then compared with the results obtained from analytical solution in Sapphire and numerical simulation in CMG as shown in **Fig. 35**. A good coherence between the estimated values can be observed. We believe that the discrepancy in the match is due to a lack of locally refined cells around the well to better model the pressure drop at the wellbore. Our current algorithm can only handle uniform grid sizes, but this limitation is being taken care of in future work, and this discrepancy will be re-examined.

After comparing the pressure results for constant well rate, the results for our proposed rate solution based on geometric approximation were calculated for a constant bottomhole pressure of 1000 psi. The comparison of these results from analytical solution and numerical solution done in Topaz has been shown in **Fig. 36**, which shows excellent results.

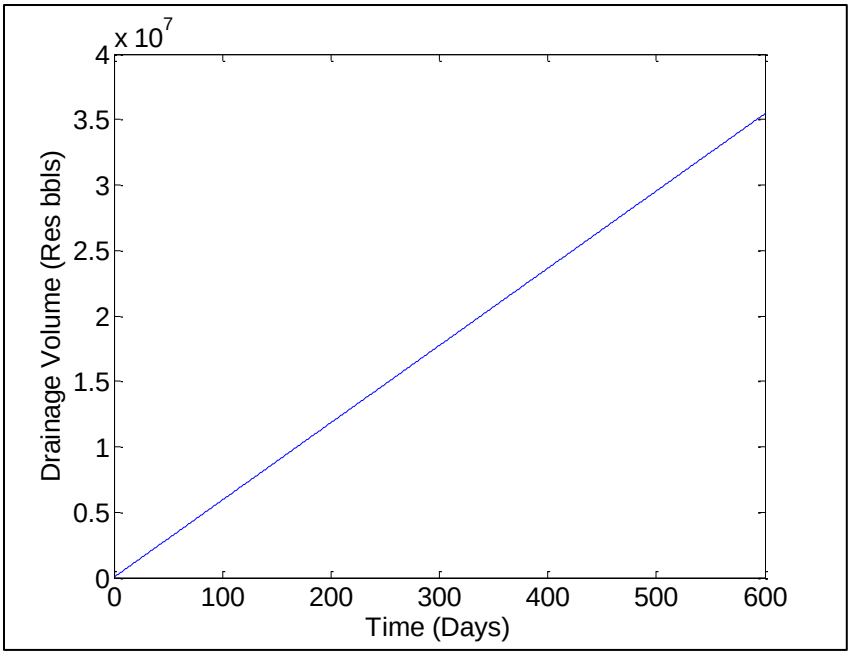

Fig. 33—Drainage volume variation for a vertical radial well in an infinite acting reservoir

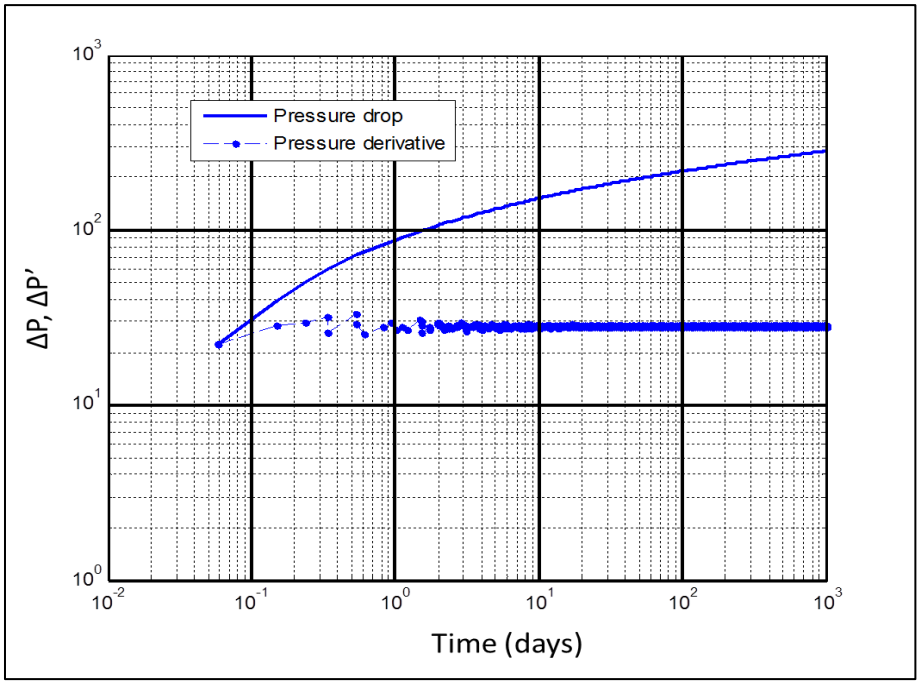

Fig. 34—Pressure drop and pressure derivative for a vertical radial well in an infinite acting reservoir

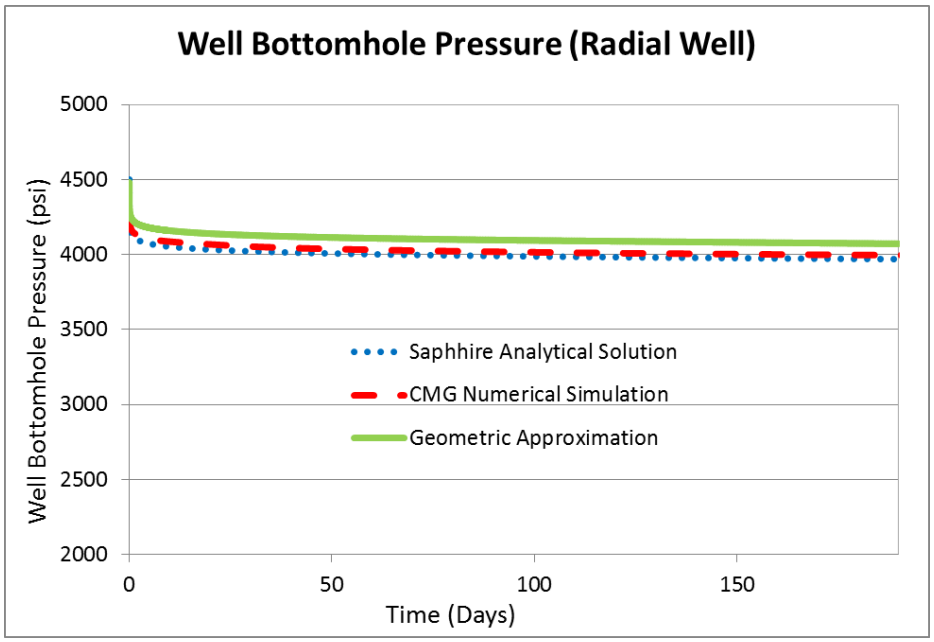

Fig. 35—Comparison of well bottomhole pressure estimated by different approaches for a vertical radial well in an infinite acting reservoir

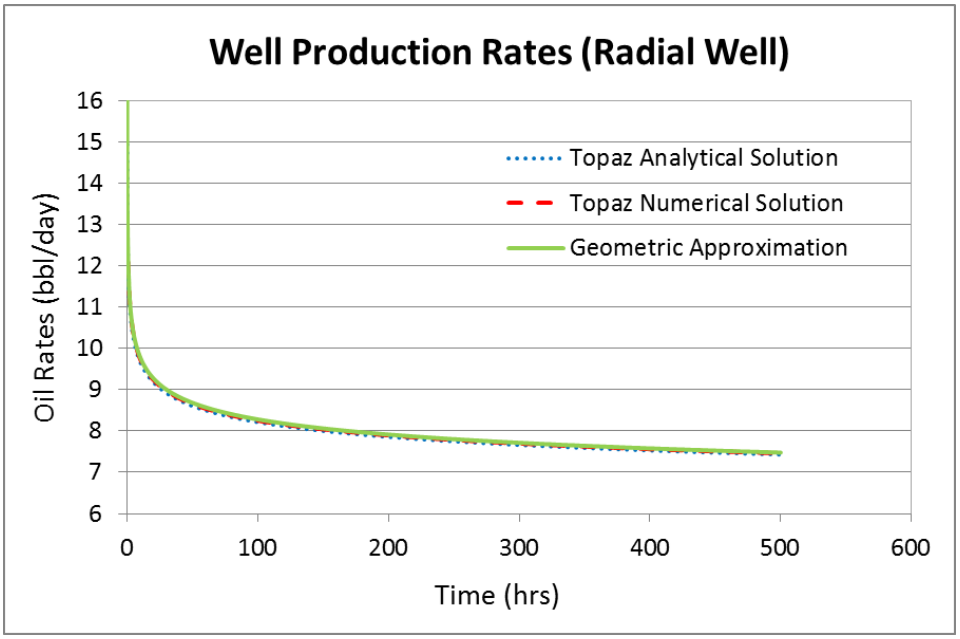

Fig. 36—Comparison of well production rates calculated by different approaches for a vertical radial well in an infinite acting reservoir

4.1.2 Single vertically fractured well in a rectangular reservoir

This is also a commonly used model for conventional reservoir study, developed with single vertical fracture to enhance the production rates. For this case, we have assumed a square shaped reservoir boundary to show the results for transient as well as boundary dominated flow. The analytical solutions for transient and boundary dominated flow in such cases have been used in the industry for a long time. For comparison purpose, we have also obtained the results from numerical simulation using CMG. **Table 6** shows the reservoir and fluid properties assumed for this case.

Table 6. Properties for a single vertically fractured well in rectangular reservoir

Property		Value	Unit
Reservoir	Porosity	0.076	fraction
	Permeability	1	md
	Thickness	10	ft
	Area	2000 X 2000	ft^2
	Initial Pressure	4100	psi
Fluid	Viscosity	0.4	cp
	Oil FVF	1	
	Total compressibility	6.00E-06	1/psi
Well / Fracture	Well radius	0.1	ft
	Fracture half-length	200	ft
	Well constant rate for pressure solution	10	bbl/day
	Well constant pressure for rate solution	1000	psi

For the case of a finite reservoir and a fractured well, the diffusive time of flight map has been shown in **Fig. 37** to show that it would follow "pill box" geometry. The drainage volume variation for this case has been shown in **Fig. 38**, where it becomes constant once all the reservoir boundaries have been reached. Then, the pressure drop and the pressure derivative were calculated for the well producing at a constant rate of 10 bbl/day, as shown in **Fig. 39**. The derivative plot clearly shows the linear flow regime at early times with a slope of half, transitioning to pseudo-radial flow regime with a slope of zero and then ultimately boundary dominated flow with a unit slope.

The calculated well bottomhole pressure based on our approach was then compared with the results obtained from analytical solution in Sapphire and numerical simulation in CMG as shown in **Fig. 40**. Similar results were obtained through the different approaches.

After comparing the pressure results for constant well rate, the results for our proposed rate solution based on the geometric approximation were calculated for a constant bottomhole pressure of 1000 psi. The comparison of these results from analytical solution and numerical solution done in Topaz has been shown in **Fig. 41**, which again shows excellent results.

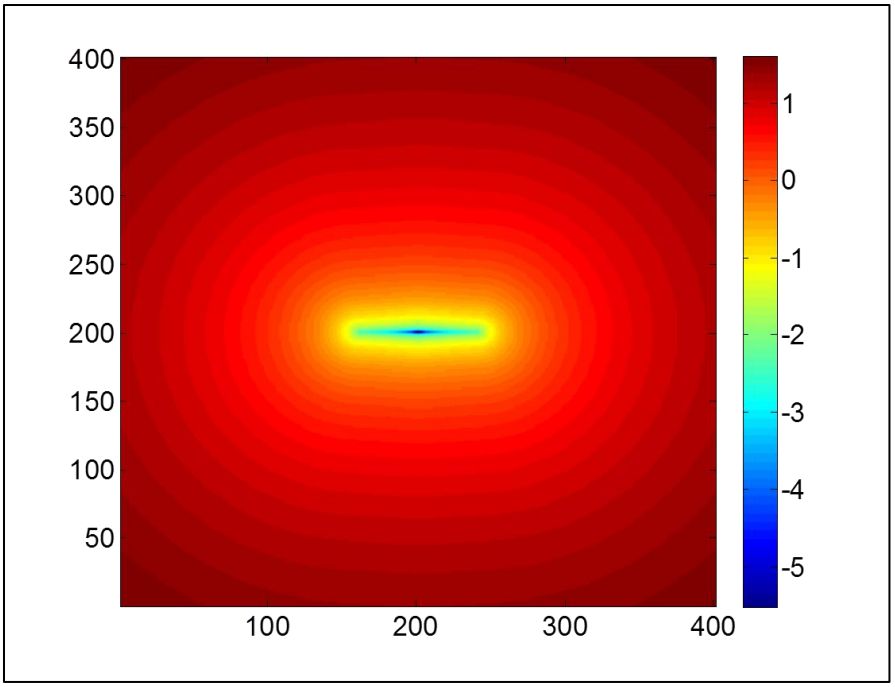

Fig. 37—Log 10 diffusive time of flight distribution for a single vertically fractured well in a rectangular reservoir

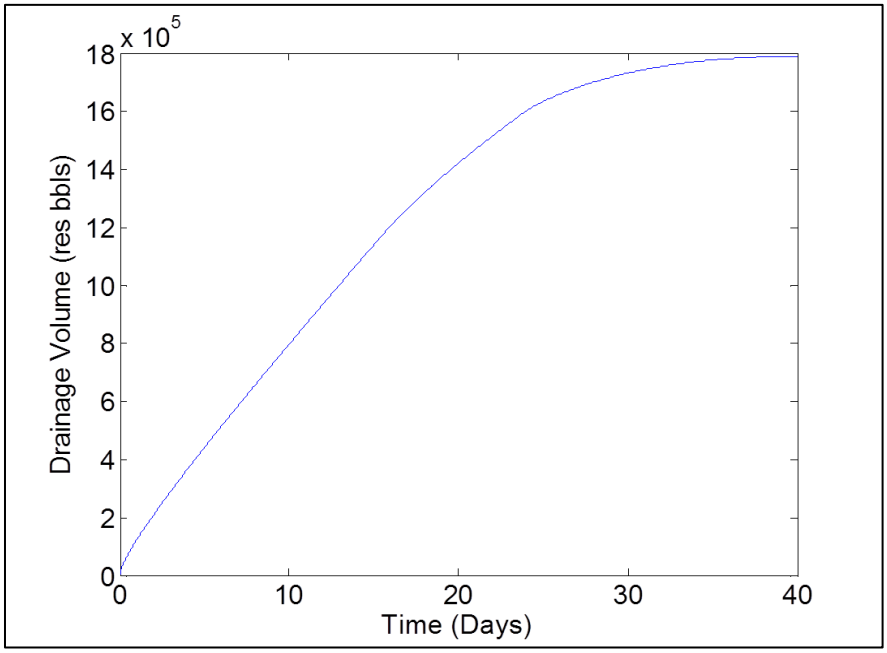

Fig. 38—Drainage volume variation for a single vertically fractured well in rectangular reservoir

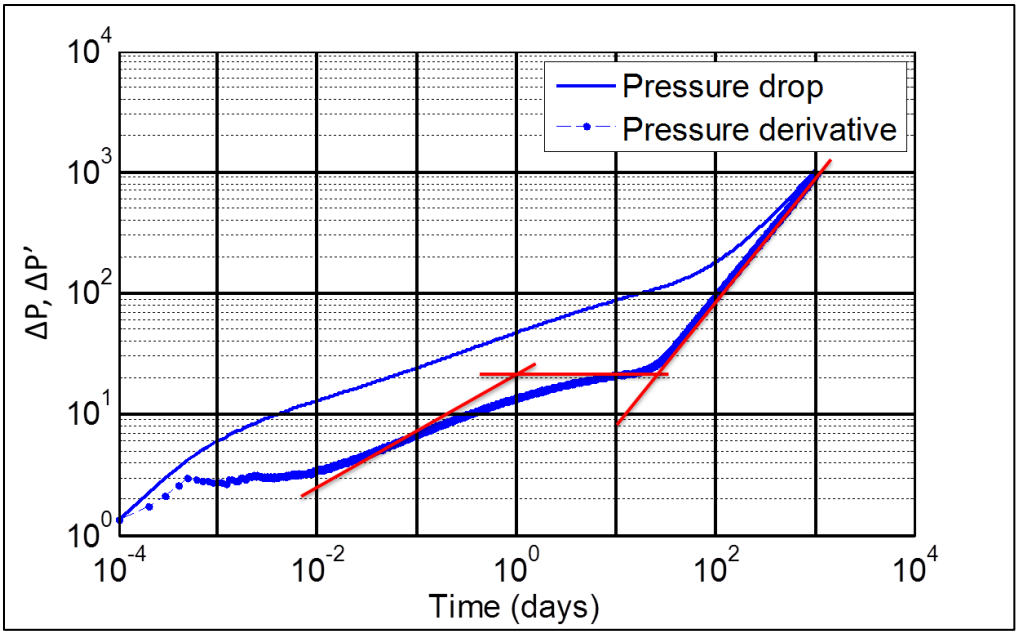

Fig. 39—Pressure drop and pressure derivative for a single vertically fractured well in a rectangular reservoir

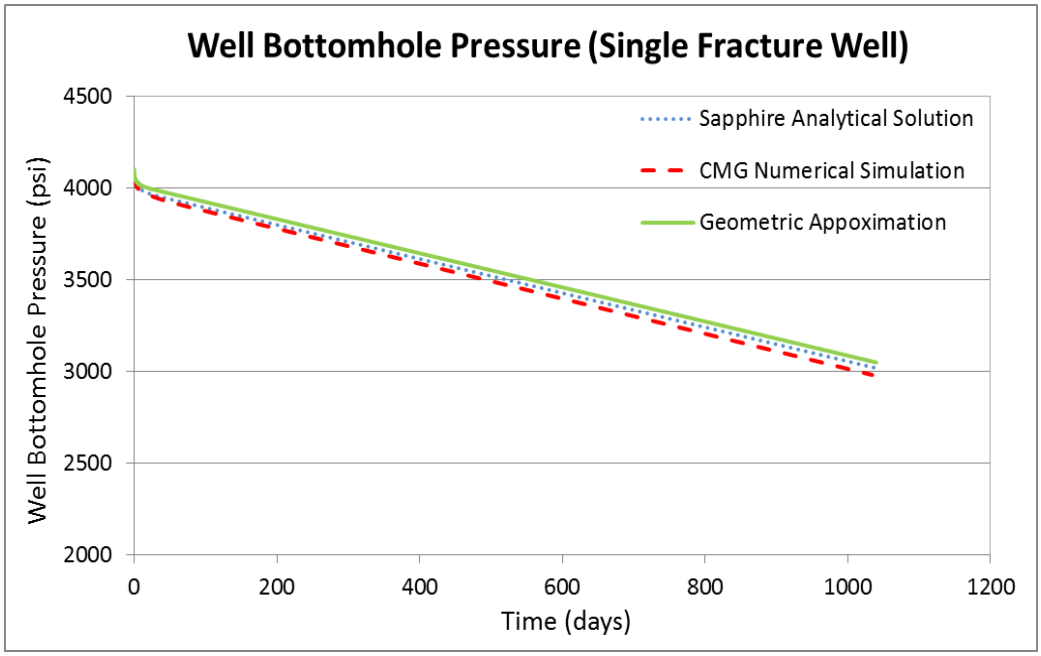

Fig. 40—Well bottomhole pressure estimated by different approaches for a single vertically fractured well in a rectangular reservoir

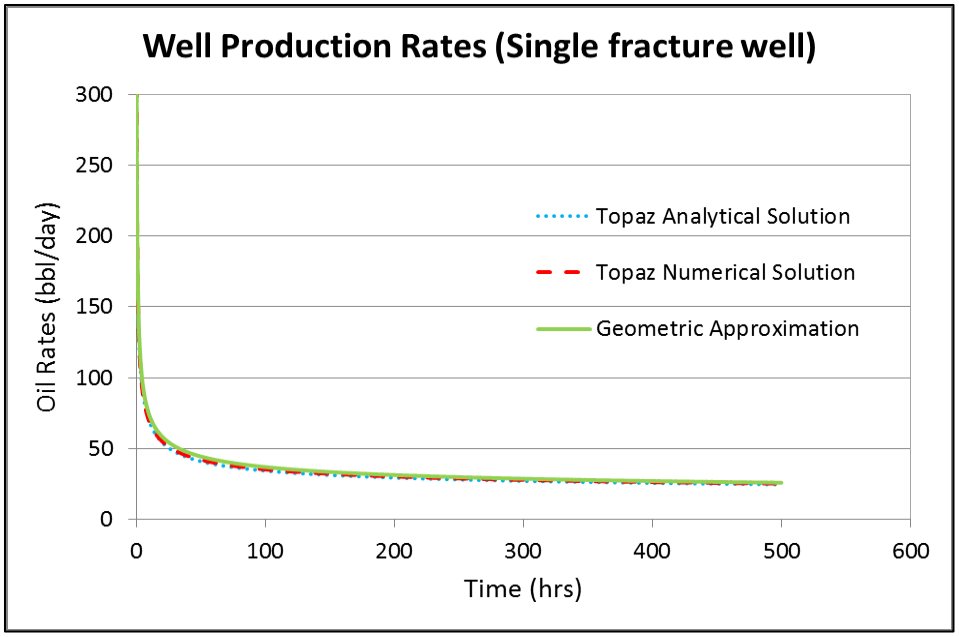

Fig. 41—Comparison of well production rates estimated by different approaches for a single vertically fractured well in a rectangular reservoir

4.1.3 Horizontal well with multiple hydraulic fractures

This is the most common model used for study of unconventional reservoirs, where the low permeability reservoir is developed with a long horizontal well, having multiple hydraulic fractures to obtain higher SRV. In such wells, the fractures can be either modeled with high (almost infinite) fracture conductivity or a finite fracture conductivity. We are including the infinite conductivity case in the homogeneous case and the finite fracture conductivity case in the heterogeneous section.

High or infinite fracture conductivity

For this case, we have assumed a constant matrix permeability of 7.5*10^-4 md, constant matrix porosity of 0.076 and very high fracture conductivity of 4000 md-ft. A

rectangular grid boundary has been assumed to show the results for transient as well as boundary dominated flow. There are no analytical solutions for transient and boundary dominated flow in such cases, so we have compared the results with numerical simulation using CMG. **Table 7** shows the reservoir and fluid properties assumed for this case.

Table 7. Properties of a horizontal well with multiple hydraulic fractures (high fracture conductivity) in a rectangular reservoir with homogeneous matrix properties

Property		Value	Unit
Reservoir	Porosity	0.076	fraction
	Permeability	7.5*10^-4	md
	Number of grids	440 X 1320 X 10	
	Grid size	4 X 4 X 4	ft^3
	Initial Pressure	4500	psi
Fluid	Viscosity	0.2	cp
	Oil FVF	1	
	Total compressibility	3.30E-05	1/psi
Well / Fracture	Well radius	0.25	ft
	Fracture half-length	480	ft
	Fracture conductivity	4*10^3	md-ft
	Well constant rate for pressure solution	12	bbl/day

For this case of almost infinite fracture conductivity and finite reservoir size, the drainage volume variation with time has been shown in **Fig. 42**. For visualization purpose, the depth of investigation at the end of 3 months, 5 years and 10 years has also been shown in **Fig. 43**. As observed in the figure, the flow is initially separate around each fracture, then interference starts between flows to different fractures and finally the whole of the SRV is depleted. These flow regimes can also be observed by plotting the

pressure derivative and pressure drop obtained from our geometric pressure solution, as shown in **Fig. 44**. This plot clearly shows the following flow regimes:

- Fracture bounded flow regime, with unit slope indicating initial flow only within the fracture;
- Linear flow regime, with a slope of half indicating flow from matrix to fractures;
- Transition flow regime after linear flow ends and where there is interference between flow to individual fractures, and then finally
- Pseudo steady flow regime indicated by unit slope when the whole SRV is being drained.

The calculated well bottomhole pressure based on our approach was then compared with the results obtained from numerical simulation in CMG as shown in **Fig. 45**. Similar results were obtained through both methods which illustrates the power of our methodology. However, in the case of multiple fractures, the limitations of a first arrival pressure approximation could be improved through the use of superposition of simpler solutions for each fracture.

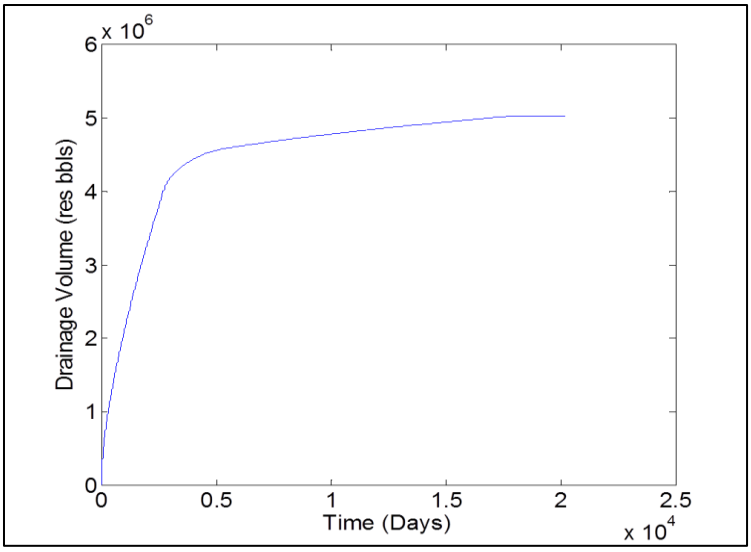

Fig. 42—Drainage volume variation for a multiple hydraulically fractured well with homogeneous matrix properties and high fracture conductivity

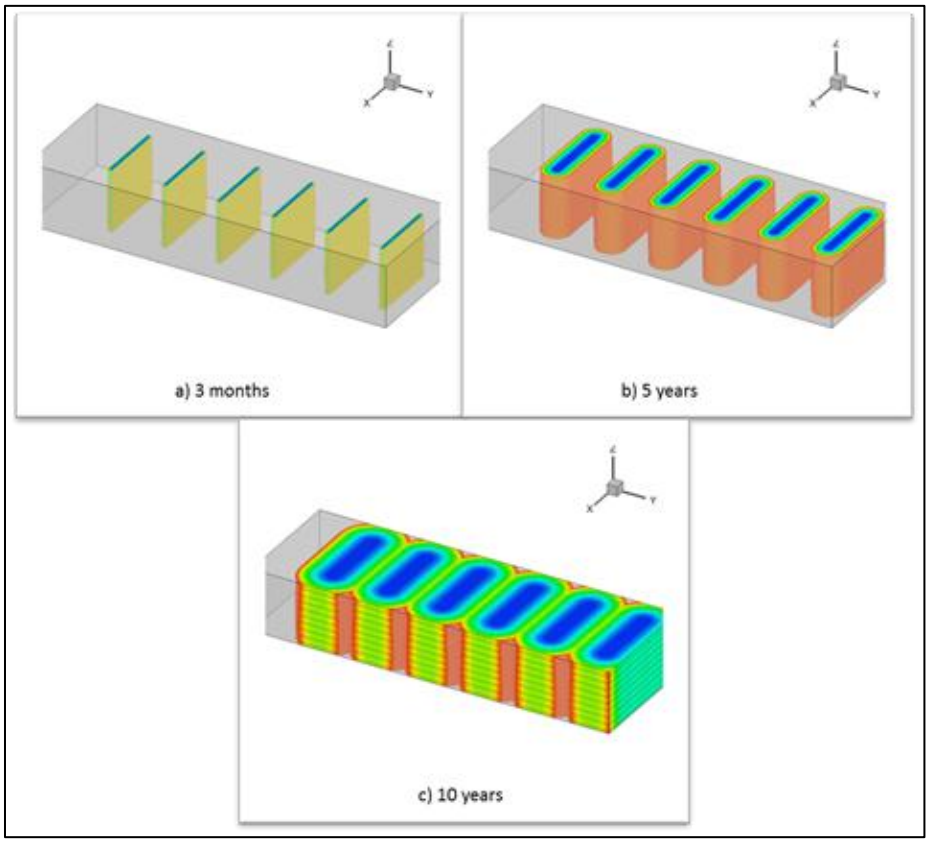

Fig. 43—Drainage volume visualizations at the end of 3 months, 5 years and 10 years for a multiple hydraulically fractured well with high fracture conductivity

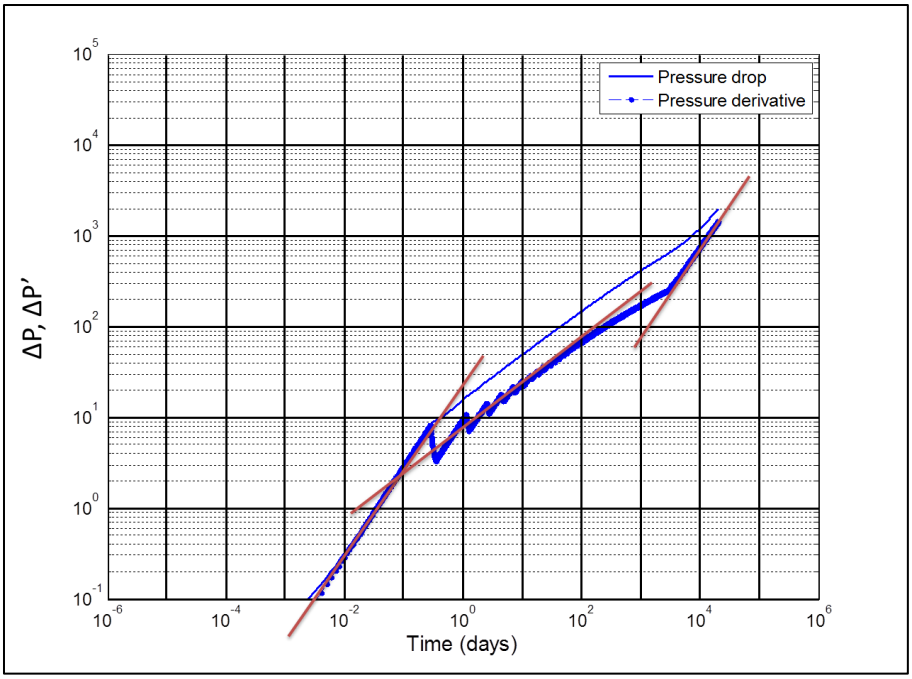

Fig. 44—Pressure drop and pressure derivative for a multiple hydraulically fractured well with high fracture conductivity

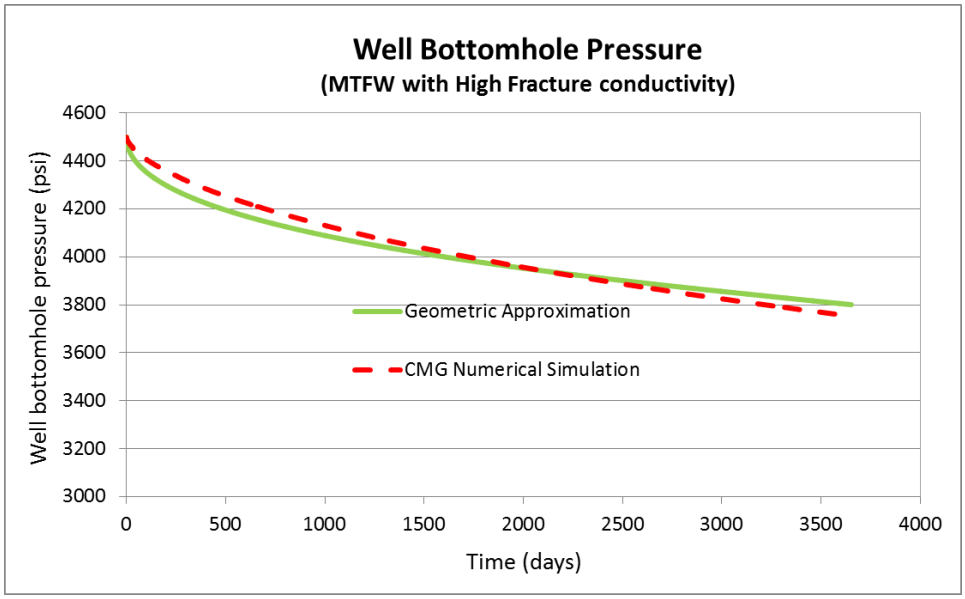

Fig. 45—Well bottomhole pressure estimated by different approaches for a single vertically fractured well in a rectangular reservoir

4.2 Heterogeneous cases

To study the application of our methodology to heterogeneous reservoirs, we have already presented a 2D example with radial well in Chapters II & III (**Fig. 19 & 20**). In this section, we have illustrated an example of a multiple transverse fractured well with finite fracture conductivity in a homogeneous reservoir and then a multiple transverse fractured well in a heterogeneous reservoir.

4.2.1 Multiple hydraulically fractured well with finite fracture conductivity

For this case, we have assumed the same properties as specified in **Table 7** except the fracture conductivity, which has been taken as 4 md-ft. Again, a rectangular grid boundary has been assumed and the results have been compared with the numerical simulation in CMG.

In such case of finite fracture conductivity, the drainage volume variation with time has been shown in **Fig. 46**. For visualization purpose, the depth of investigation at the end of 0.25 hours, 2.5 days, 5 months and 30 years has also been shown in **Fig. 47**. The pressure derivative and pressure drop response was also generated as shown in **Fig. 48**, and the following flow regimes can be interpreted from the pressure derivative plot:

- Early linear flow within the fracture, with a slope of half,
- Pseudo radial flow regime around the well, with a slope trending towards zero,
- Transition flow regime where the flow becomes almost elliptical and then finally,

- Pseudo steady flow regime indicated by unit slope when the whole SRV is being drained.

The calculated well bottomhole pressure based on our approach was then compared with the results obtained from numerical simulation in CMG as shown in **Fig. 49**. Similar results were obtained through both methods. Interestingly, **Fig. 49** shows better correspondence with numerical simulation than does **Fig. 48**, which warrants additional investigation.

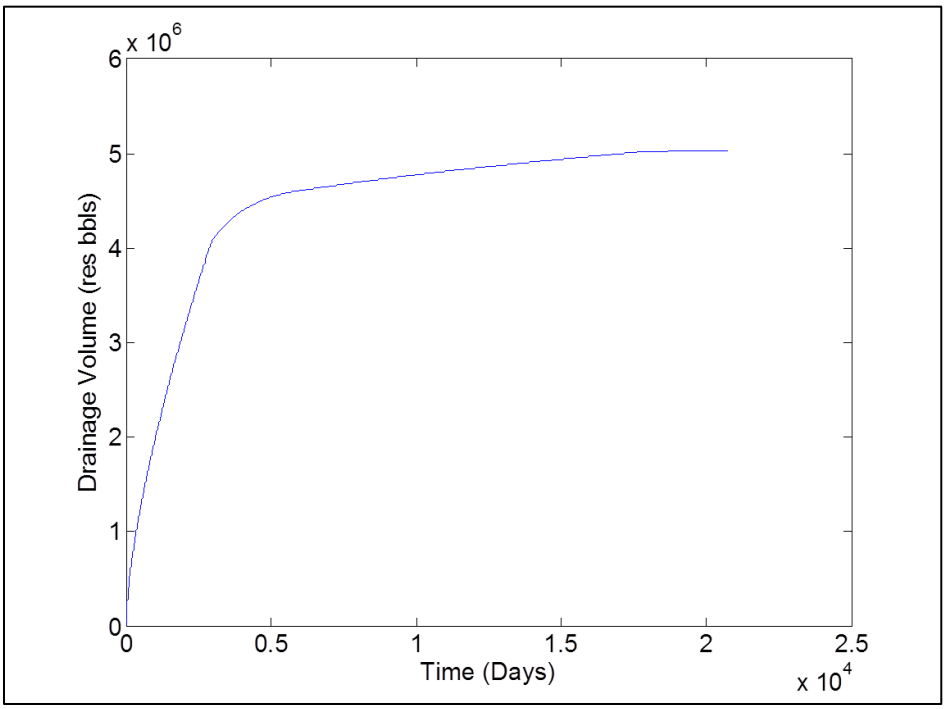

Fig. 46—Drainage volume variation for a multiple hydraulically fractured well with finite fracture conductivity

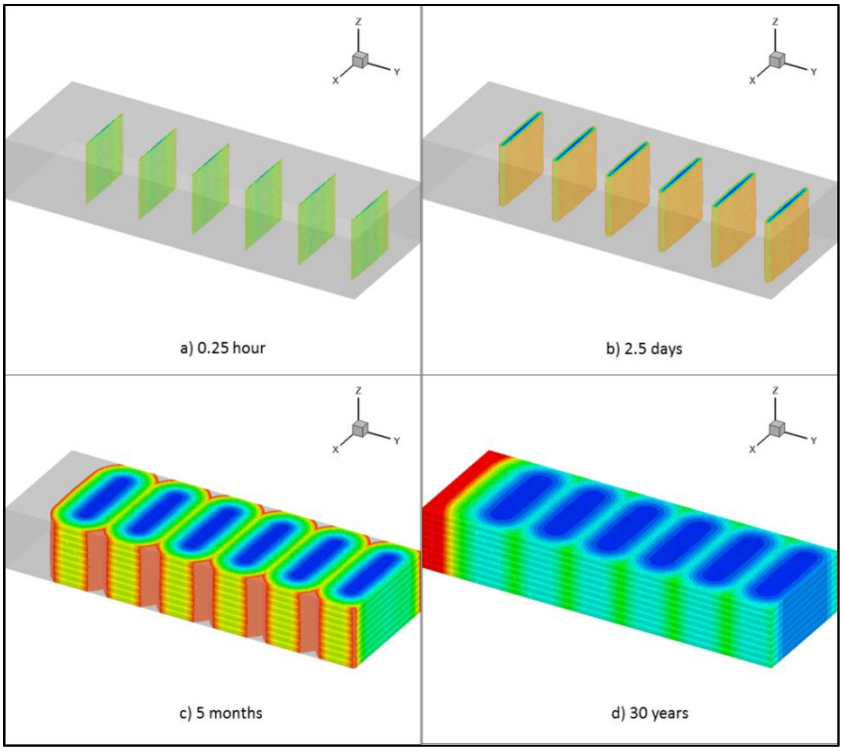

Fig. 47—Visualizations for the depth of investigation at the end of 0.25 hours, 2.5 days, 5 months and 30 years

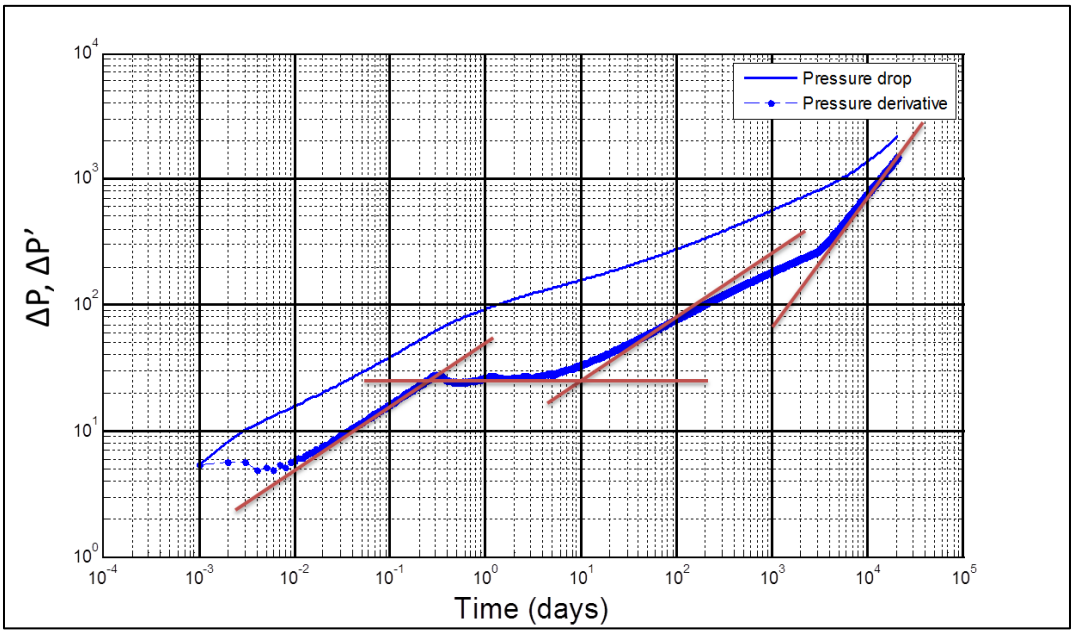

Fig. 48—Pressure drop and derivative for a multiple hydraulically fractured well with finite fracture conductivity and homogeneous reservoir properties

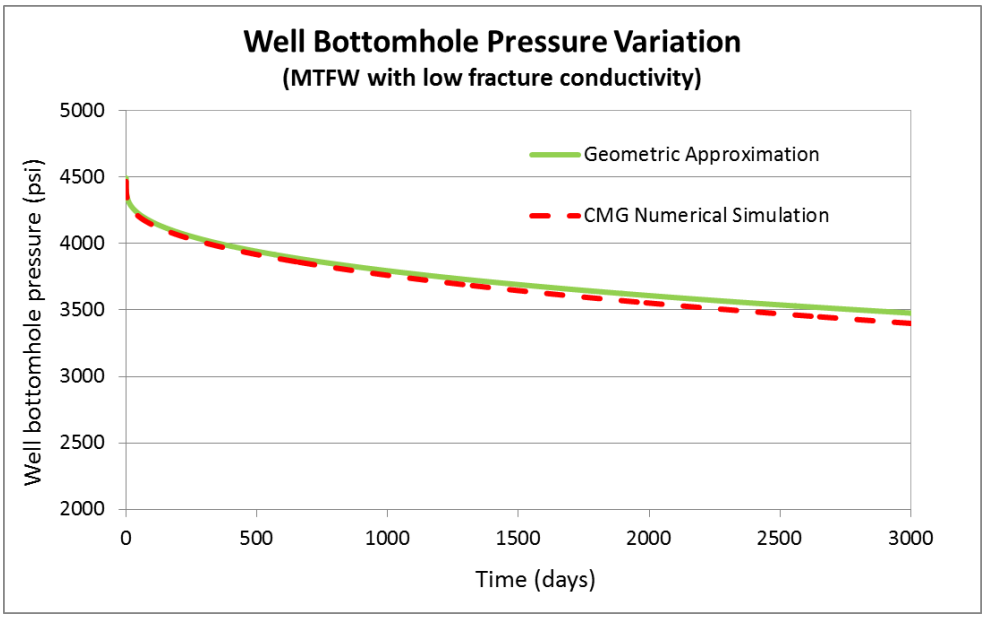

Fig. 49—Comparison of well bottomhole pressure by different approaches for a multiple hydraulically fractured well with finite conductivity

4.2.2 Multiple hydraulically fractured well in a heterogeneous reservoir

In this section, we will study a multiple hydraulically fractured well producing from a heterogeneous reservoir (Xie et al. 2012). The matrix permeability lies in the range of 10^-5 md to 10^-2 md. A distribution map with the log of permeability has been shown in **Fig. 50**. A fracture permeability of 1 md has been assumed.

The drainage volume variation estimated by the FMM approach for this case has been shown in **Fig. 51**. The visualization for the depth of investigation at the end of 1 day, 10 days, 5 months and 30 years is depicted in **Fig. 52**, which shows more scatter than observed for the homogeneous case. **Fig. 53** presents the estimated pressure drop and

pressure derivative for a constant production rate of 13.2 bopd. The pressure derivative roughly indicates the following flow regimes:

- Linear flow within the fracture, with a slope of half,
- Pseudo-radial flow, for a very small period though,
- Transition flow, when the flow gets distorted due to heterogeneity, giving no distinct slope, and then finally,
- Pseudo steady flow, with a unit slope, where the whole reservoir is being drained.

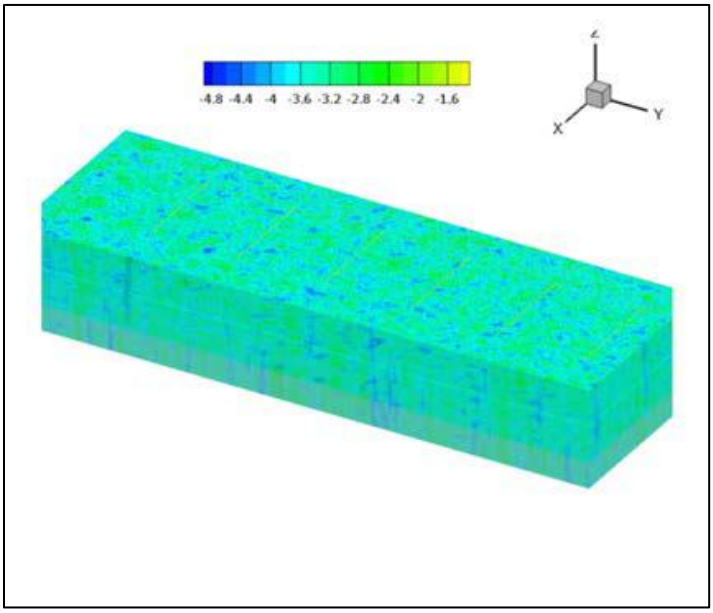

Fig. 50—Distribution of log permeability for the heterogeneous reservoir system

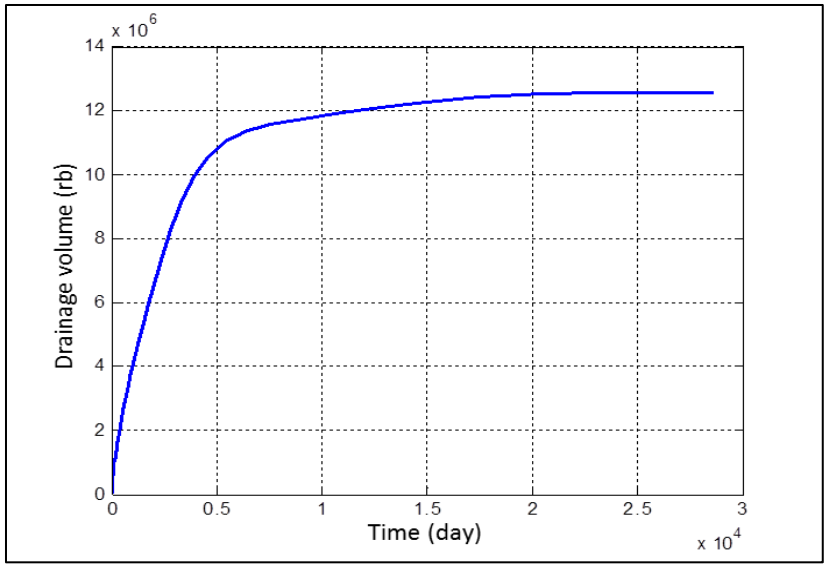

Fig. 51—Drainage volume variation for a heterogeneous matrix with multiple hydraulically fractured well

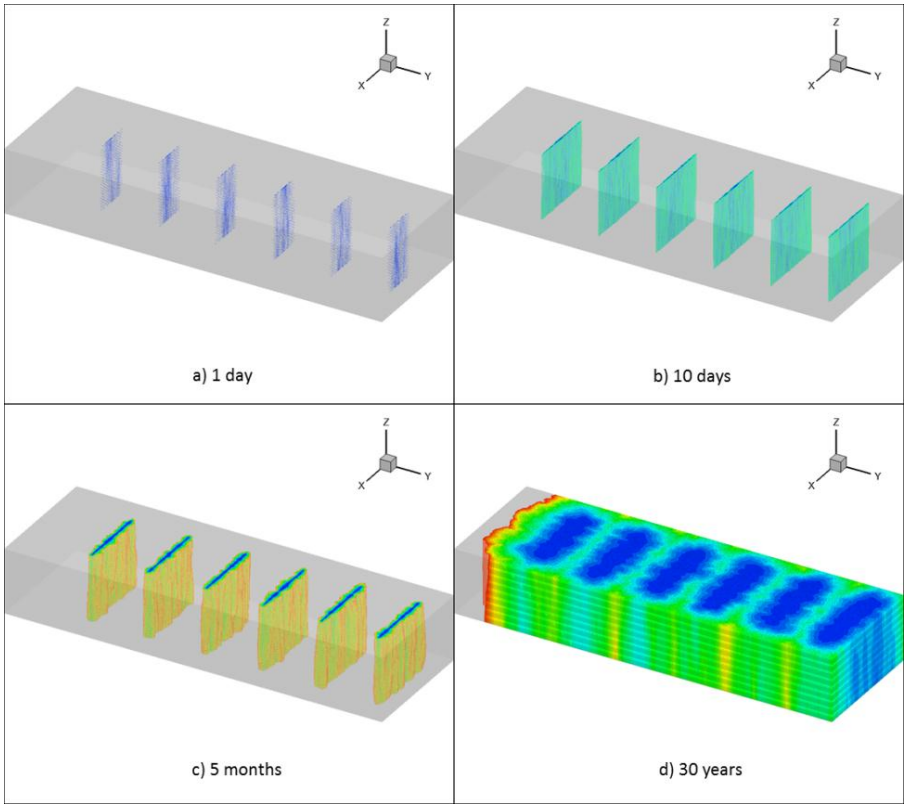

Fig. 52—Visualizations for the depth of investigation at the end of 1 day, 10 days, 5 months and 30 years.

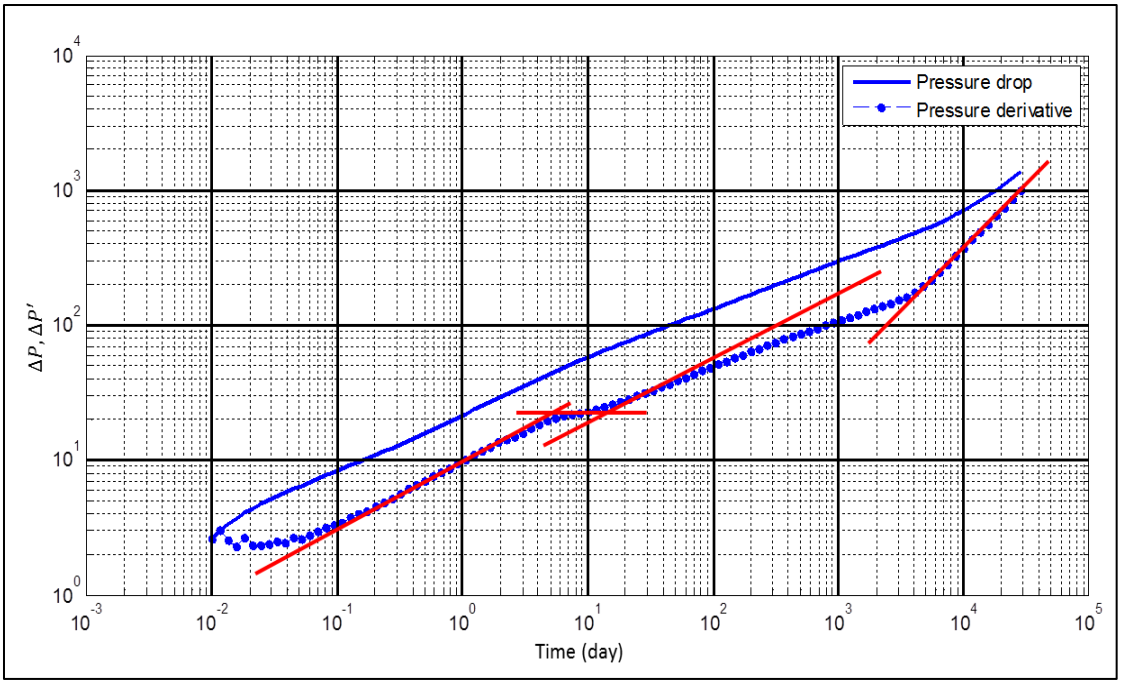

Fig. 53—Pressure drop and pressure derivative for a heterogeneous reservoir with multiple hydraulically fractured well

4.3 Discussion of results

As observed in the results above for homogeneous and heterogeneous cases, the geometric solution is suitable for all the general cases and provides similar results to those obtained from analytical and numerical solutions. The flow regimes obtained from the pressure response are the same observed by other authors (Al-Kobaisi et al. 2006; Song et al. 2011). Thus, the current approach provides a general methodology for studying a wide variety of reservoir and well types, including complex fracture geometries, presence of natural fractures, variable fracture conductivities. In summary, this solution can handle any reservoir heterogeneity which can be defined for a gridded system.

CHAPTER V

CONCLUSIONS

5.1 Summary and conclusions

This thesis demonstrates a novel technique developed for estimating drainage volumes and predicting pressure depletion and production rate behavior at all flow times for a general reservoir system. This methodology is unique and the first semi-analytical approach with wide applicability including heterogeneous property distribution, complex well geometry and bounded/semi-bounded reservoir geometry. The main concepts and learnings from the proposed methodology can be summarized as below:

- The radius of investigation for a radial well in a homogeneous reservoir is dependent on the flow type, and can be generalized for any radially symmetric flow. The well bottomhole pressure and flux solutions can also be generalized for such flow types by using an incomplete gamma function.
- The pressure front propagation in any reservoir follows an Eikonal equation obtained from an asymptotic solution of the diffusivity equation. This equation can be solved for heterogeneous reservoirs, by using a very efficient 'Fast Marching Method' algorithm. This algorithm provides a diffusive time of flight distribution away from the source, providing the 'depth of investigation' of the pressure front at all flow times.

- The diffusive time of flight calculation provides the pressure front location at any time and the encompassed reservoir volume can be estimated as the drainage volume.
- For a well producing at constant production rates, the pressure depletion at any location in the reservoir can be estimated by applying a geometric approximation based on the estimated drainage volumes. This approximation can also be extended to wells producing at constant bottomhole pressure, for obtaining the flux solution at any location in the reservoir.
- While applying the geometric pressure and flux solutions, the integration should be done over the boundaries related to the asymptotic pressure and flux solutions, which are not necessarily the same as the depth of investigation.
- The geometric pressure solution is based on the first wave arrival concept and the contrast in the reservoir properties in heterogeneous reservoirs should be taken into consideration when applying this approximation.

By applying this methodology to various cases, we have demonstrated that the results are consistent with previous analytical solutions and numerical simulation, and require much less computation time. It can also provide a quick visualization for the depth of investigation and can help identify the different flow regimes. In the thesis, we have shown that this approach can be especially useful for unconventional reservoir studies, where no analytical solutions are available for multiple transverse hydraulically fractured wells. The rapid but approximate results from this solution can be extremely

helpful for well or fracture design, history matching calibration, reservoir management and optimization studies.

5.2 Future work

The results obtained from the suggested methodology are very encouraging. However, the solution is still early in its development and has scope for improvements. Some of the identified areas requiring further work are:

- Modification of the algorithm to handle variable grid sizing in the reservoir, like local grid refinements or corner point cell geometries to widen the applicability of the approach and to provide better approximation results.
- Additional studies at early time to better understand some of the near well discrepancies seen compared to simulation.
- Adjusting the solution to handle variable compressibility, especially for studying gas reservoirs. This might include addition of correlations for calculating gas compressibility and viscosity with changes in pressure to estimate pseudo-pressures and material balance times.
- Extending the algorithm to include the calculation of flow cross sectional area at all times, similar to drainage volume calculations, to apply the proposed flux solution for heterogeneous reservoirs.
- Studies of the long time transients and the relationship with the steady state solutions.
- Development of a sensitivity based approach to pressure history matching.

These areas are currently being worked on by other graduate students in the MCERI research group and would hopefully extend the current solution for other utilities and applications.

REFERENCES

Agarwal, R.G. 2010. Direct Method of Estimating Average Reservoir Pressure for Flowing Oil and Gas Wells. In *SPE Annual Technical Conference and Exhibition*. Florence, Italy: Society of Petroleum Engineers, 19-22 September, SPE-135804-MS.

Al-Kobaisi, M., Ozkan, E., Kazemi, H. et al. 2006. Pressure-Transient-Analysis of Horizontal Wells with Transverse, Finite-Conductivity Fractures. In *Canadian International Petroleum Conference*. Calgary, Alberta: Petroleum Society of Canada, 13-15 June, PETSOC-2006-162.

Bello, R.O. and A, W.R. 2010. Multi-Stage Hydraulically Fractured Horizontal Shale Gas Well Rate Transient Analysis. In *North Africa Technical Conference and Exhibition*. Cairo, Egypt: Society of Petroleum Engineers,14-17 February, SPE-126754-MS.

Cinco-Ley, H. and Samaniego-V, F. 1981. Transient Pressure Analysis for Fractured Wells. *SPE Journal of Petroleum Technology* **33** (9): 1749-1766.

Datta-Gupta, A. and King, M.J. 2007. *Streamline Simulation: Theory and Practice*. SPE Textbook Series. 222, Palisades Creek Drive, Richardson, TX, 75080-2040 USA: Society of Petroleum Engineers. Original edition.

Datta-Gupta, A., Xie, J., and Gupta, N. 2011. Radius of Investigation and Its Generalization to Unconventional Reservoirs. *Journal of Petroleum Technology* **63** (7): 52-55.

Fetkovich, M.J. 1980. Decline Curve Analysis Using Type Curves. *SPE Journal of Petroleum Technology* **32** (6): 1065-1077, SPE- 00004629.

Hsieh, B.Z., Chilingar, G.V., and Lin, Z.S. 2007. Propagation of Radius of Investigation from Producing Well. *Energy Sources, Part A: Recovery, Utilization, and Environmental Effects* **29** (5): 403-417.

Kang, S., Datta-Gupta, A., and Lee, W.J. 2011. Impact of Natural Fractures in Drainage Volume Calculations and Optimal Well Placement in Tight Gas Reservoirs. In *North American Unconventional Gas Conference and Exhibition*. The Woodlands, Texas, USA: Society of Petroleum Engineers, 14-16 June 2011, SPE-144338-MS.

Kuchuk, F.J. 2009. Radius of Investigation for Reserve Estimation from Pressure Transient Well Tests. In *SPE Middle East Oil and Gas Show and Conference*.

Bahrain, Bahrain: Society of Petroleum Engineers, 15-18 March 2009, SPE-120515-MS.

Lee, W.J. 1982. *Well Testing*. SPE Textbook Series. Richardson, TX: Society of Petroleum Engineers. Original edition.

Mandelbrot, B.B. 1982. *The Fractal Geometry of Nature*. USA Original edition.

Meyer, B.R., Bazan, L.W., Jacot, R.H. et al. 2010. Optimization of Multiple Transverse Hydraulic Fractures in Horizontal Wellbores. In *SPE Unconventional Gas Conference*. Pittsburgh, Pennsylvania, USA: Society of Petroleum Engineers, 23-25 February 2010, SPE-131732-MS.

Nordbotten, J.M., Celia, M.A., and Bachu, S. 2004. Analytical Solutions for Leakage Rates through Abandoned Wells. *Water Resour. Res.* **40** (4): W04204.

Oliver, D. 1994. Application of a Wave Transform to Pressure Transient Testing in Porous Media. *Transport in Porous Media* **16**: 209-236.

Raghavan, R., Cady, G.V., and Ramey, H.J. 1972. Well Test Analysis for Vertically Fractured Wells. *Journal of Petroleum Technology* (August, 1972).

Riley, M.F., Brigham, W.E., and Horne, R.N. 1991. Analytic Solutions for Elliptical Finite-Conductivity Fractures. In *SPE Annual Technical Conference and Exhibition*. Dallas, Texas: Society of Petroleum Engineers, 6-9 October 1991. SPE - 00022656.

Sethian, J.A. 1999. Level Set Methods and Fast Marching Methods. *Cambridge University Press, New York City*.

Sethian, J.A. and Vladimirsky, A. 2000. Fast Methods for the Eikonal and Related Hamilton– Jacobi Equations on Unstructured Meshes. *Proceedings of the National Academy of Sciences* **97** (11): 5699-5703.

Song, B., Economides, M.J., and Ehlig-Economides, C.A. 2011. Design of Multiple Transverse Fracture Horizontal Wells in Shale Gas Reservoirs. In *SPE Hydraulic Fracturing Technology Conference*. The Woodlands, Texas, USA: Society of Petroleum Engineers, 24-26 January 2011, SPE-140555-MS.

Vasco, D., Keers, H., and Harasaki, K. 2000. Estimation of Reservoir Properties Using Transient Pressure Data: An Asymptotic Approach. *Water Resources Research* **36** (12): 3447-3465.

Virieux, J., Flores-Luna, C., and Gilbert, D. 1994. Asymptotic Theory for Diffusive Electromagnetic Imaging. *Geophysics J. Int.* **119**: 857-868.

Xie, J., Gupta, N., King, M.J. et al. 2012. Depth of Investigation and Depletion Behavior in Unconventional Reservoirs Using Fast Marching Methods. In *SPE Europec/EAGE Annual Conference*. Copenhagen, Denmark: Society of Petroleum Engineers, SPE-154532-MS.